Lappeenranta University of Technology
Faculty of Technology
Degree Programme in Energy Technology

Nikita Ivankov

Analysis of PWR-PACTEL Small Break LOCA experiment using TRACE

Examiners: Prof. Dr. Juhani Hyvärinen

Supervisors: Dr. Juhani Vihavainen

ABSTRACT

Lappeenranta University of Technology
Faculty of Technology
Degree Programme in Energy Technology

Nikita Ivankov

Analysis of PWR PACTEL Small Break LOCA experiment using TRACE

Master's Thesis

78 pages, 43 figures, 8 tables,

Examiners: Prof. Dr. Juhani Hyvärinen
Dr. Juhani Vihavainen

Keywords: Thermal-hydraulic system codes, Loss-Of-Coolant Accident (LOCA), TRACE, PWR PACTEL facility, Stepwise inventory reduction experiment, Small break LOCA experiment.

Currently, the power generation is one of the most significant life aspects for the whole mankind. Barely one can imagine our life without electricity and thermal energy. Thus, different technologies for producing those types of energy need to be used. Each of those technologies will always have their own advantages and disadvantages. Nevertheless, every technology must satisfy such requirements as efficiency, ecology safety and reliability. In the matter of the power generation with nuclear energy utilization these requirements needs to be highly maintained, especially since accidents on nuclear power plants may cause very long term deadly consequences. In order to prevent possible disasters related to the accident on a nuclear power plant strong and powerful algorithms were invented in last decades. Such algorithms are able to manage calculations of different physical processes and phenomena of real facilities. However, the results acquired by the computing must be verified with experimental data.

ACKNOWLEDGEMENTS

The work was done within Lappeenranta University of Technology. I want to say thank you to my proximate supervisors Prof. Dr. Juhani Hyvärinen and Dr. Juhani Vihavainen. I am very grateful to the LUT administrations. Thanks to LUT for giving me the opportunity to open my mind.

TABLE OF CONTENTS

1 INRODUCTION 9

1.1. Background of the thesis 10

1.2. Goals and structure of the thesis 12

2 PWR PACTEL FACILITY DESCRIPTION 13

2.1. General 13

2.1.1. Pressure vessel model and core components 15

2.1.2. Primary loops 18

2.1.3. Main circulation pumps 19

2.1.4. Steam generators 19

2.1.5. Pressurizer 22

2.1.6. Emergency core cooling systems 22

2.1.7. Water treatment and start up procedures 23

2.2. Design and scaling principles 23

2.2.1. Design principles 23

2.2.2. Scaling approach 25

2.3. Instrumentation 27

2.3.1. Temperature acquisitions 27

2.3.2. Pressure measurements 30

2.3.3. Differential pressure measurements 30

2.3.4. Flow rate meters 30

2.3.5. Core heating power 30

3 TRACE CODE OVERVIEW 31

3.1. TRACE Characteristics 32

3.2. Physical phenomena considered 32

3.3. Limitations on use 33

3.4. Field Equations 34

4 TRACE MODEL OF PWR PACTEL FACILITY 40

4.1. Primary side 41

4.2. Secondary side 42
5 EXPERIMENTS DESCRIPTION 44
5.1. Natural circulation 44
5.2. Stepwise Inventory Reduction experiments 46
5.2.1. SIR-31 47
5.2.2. SIR-32 48
5.2.3. SIR-33 48
5.3. Small Break LOCA experiment 49
5.3.1. SBL-50 49
6 CALCULATION RESULTS 50
6.1. Stepwise Inventory Reduction experiments 50
6.1.1. SIR-31 51
6.1.2. SIR-32 57
6.1.3. SIR-33 63
6.2. Small Break LOCA experiment 68
6.2.1. SBL-50 68
7 CONCLUSIONS AND DISCUSSION OF THE RESULTS 75
BIBLIOGRAPHY 77

NOMENCLATURE

Roman

C = shear coefficient

E_i = rate of energy transfer per unit volume across phase interfaces

e = internal energy

f = force per unit volume

$\vec{g}$ = gravity vector

h = heat-transfer coefficient (HTC)

$h_{w,}$ = the effective wall HTC to gas

h_w = the effective wall HTC to liquid

h_l' = liquid enthalpy of the bulk liquid if the liquid is vaporizing or the liquid saturation enthalpy if vapor is condensing

h_v' = vapor enthalpy of the bulk vapor if the vapor is condensing or the vapor saturation enthalpy if liquid is vaporizing

M_i = rate of momentum transfer per unit volume across phase interfaces

P = fluid pressure or total pressure

q = heat-transfer rate per unit volume

q_d = power deposited directly to the gas or liquid (without heat-conduction process)

q' = heat flux

r = radius

t = time

T = temperature

T = stress tensor

T_{sv} = saturation temperature corresponding to the vapor partial pressure

$\vec{V}$ = velocity vector

V = magnitude of the velocity

z = axial coordinate

Greek

α = gas volume fraction

Γ = interfacial mass-transfer rate (positive from liquid to gas)

ρ = density

θ = inclination angle from vertical or the azimuthal coordinate

Subscripts

d = denotes direct heating when used with energy source (q)

g = gas mixture

i = interfacial

l = liquid

v = water vapor

w = wall

LIST OF SYMBOLS AND ABBREVIATIONS

BWR	Boiling Water Reactor
CCFL	Counter-Current Flow Limitation
DEGB	Double-Ended Guillotine Break
ECCS	Emergency Core Cooling System
EPR	European Pressurized water Reactor
ESBWR	Economic Simplified Boiling Water Reactor
HPIS	High Pressure Injection System
HTC	Heat-Transfer Coefficient
LB LOCA	Large Break Loss-Of-Coolant Accidents
LOCA	Loss Of Coolant Accidents
LPIS	Low Pressure Injection System
LUT	Lappeenranta University of Technology
LWR	Light Water Reactor
Ni cFP	National Instruments Compact FieldPoint
NPP	Nuclear Power Plant
NTC	Negative Temperature Coefficient
PACTEL	Parallel channel test facility
PDE	Partial Differential Equation
PWR	Pressurized Water Reactor
RTD	Resistance Temperature Detectors
SB LOCA	Small Break Loss-Of-Coolant Accidents
SBL	Small Break LOCA experiments
SIR	Stepwise Inventory Reduction experiments
VVER	Vodo Vodyanoy Energeticheskiy Reaktor

1 INRODUCTION

Now electrical power generation is one of the most vital tasks. There are several possible policy menus to this problem such as thermal, hydro-, nuclear power generation in concert with renewable sources of energy. One of the most widely used principal approaches is nuclear power generation. The technology in question has its own advantages and disadvantages in comparison with the other types of power generation.

The basic principle of producing electricity by nuclear energy is transfer of heat resulting from fission reaction of fissile fuel to heat carrier medium after which either uses it directly in a turbine in order to converse heat energy of working medium to mechanical work of turbine rotor or use an intermediate recuperative heat exchanger. A number of conceptually different configurations of nuclear reactors were developed retrospectively. Among them, there are such reactors as Light Water Reactors (LWRs). This type of reactors has its own division on Pressurized Water Reactor (PWR) and Boiling Water Reactor (BWR). Both of these subclasses of LWR utilize ordinary water by way of coolant and moderator to the end that to avoid overheating of fuel and to decrease energy of released fast neutrons to thermal region in order to increase probability of new fissions.

Utilization of nuclear energy is highly attractive for a variety of reasons. For producing equal amount of thermal energy the consumption of nuclear fuel by contrast with fossil fuel is less by several orders of magnitude. Absence of carbon and nitrogen emissions makes nuclear energy relatively clean for the environment. Nevertheless, storage of nuclear waste is of immediate interest problem. Essential issue of nuclear power generation is possible catastrophic release of radioactive fission products, which can cause either short or long-term consequences, highly harmful for health of people and nearby environment.

Thus, in order to gain advantage of nuclear energy production and to reduce probability of disastrous consequences in case of an emergency, preventive systems and procedures must be applied. In developing of more accurate and objective safety systems there must be better understanding of processes taking place during a specific failure situation.

1.1. Background of the thesis

For the purpose of deflection fatal situation on Nuclear Power Plant (NPP) assumptions of maximum credible accidents must be made. The assumptions must be based on gathered experience of exploitation of NPP or be supported by objective reasons. However, inasmuch as an operating NPP cannot be a facility to investigate modes of operating leading to severe consequences, therefore other admissible solution must be found.

One of possible paths to examine peculiar phenomena inherent to ongoing processes of NPP facilities is scale modelling of those. Such method of investigation allows researchers to observe the most complex processes without endanger of environment. In reference to thermal hydraulic aspects nuclear fuel as a source of heat can be easily substitute with electrical source of energy, thereby empower to eliminate the probability of contamination by radioactive fission products. The scale modelling of thermal hydraulics of NPP provide wide range of possibilities for a researcher to study different accident situations. However, such method is one of the most cost-intensive types of approach. Development of computer-aided technologies gave an option of analyzing of diverse phenomena on qualitatively different level.

By such manners, since 70's brisk growth of thermal hydraulic system codes began. The major subject for examination was triggered by formulated Code of Federal Regulations, videlicet by § 50.46 Acceptance criteria for emergency core cooling systems for light-water nuclear power reactors (NUCLEAR REGULATORY COMMISSION. 2014). Initially, the main emphasis of research was on Large Break Loss-Of-Coolant Accidents (LB LOCAs) with Double-Ended Guillotine Break (DEGB) of primary coolant circuit which led to fast heating in most LWRs. Underlying concept consisted in that if a reactor core with Emergency Core Cooling System (ECCS) are able to experience the rapid heat up without failure, then other destructions will have less significant consequences. Therefore, first system codes concentrated on the rapid blowdown and reflood phases of the accidents (Hyvärinen 2015).

Notwithstanding, according to risk studies an apprehension appeared that in comparison with LB LOCA, small breaks would be much more likely to happen (Rasmussen 1975). From the standpoint of probabilistic risk assessment presence of medium and small-bore piping and

welds is dominating over large size piping making accidental situation more probable from Small Break Loss-Of-Coolant Accidents (SB LOCAs). Witness of that a small break can cause severe core damage served Three Mile Island Accident (Hyvärinen 2015). Unhasty piecemeal attenuation of primary coolant and absence of capability for decay heat removal by natural circulation, which were not taken into account in thermal hydraulic system models by that time (United States Nuclear Regulatory Commission 2015).

Consequently, change in research direction befell sideward of SB LOCAs after which new facilities were created together with new generation of thermal system codes. Basically, new thermal -hydraulic codes were developed by all nations utilizing nuclear energy. With the course of time, the codes developed further and were by nature of two-fluid, six-equation flow models with one-dimensional representation of space. As an example of such codes currently used American thermal hydraulic system code TRACE can serve. This code has its own features.

In Lappeenranta University of Technology (LUT), in 1976 experimental part of thermal hydraulics of NPP research began. Since then numerous experiments with reference to LWRs were implemented. Among facilities created and utilized for all of the experiments mentioned above there is the largest one, named the parallel channel test facility (PACTEL) (Purhonen 2006). The facility was designed for modelling of thermal hydraulic behavior of Vodo Vodyanoy Energeticheskiy Reaktor (VVER)-440 reactors. PACTEL has undergone several modifications and upgrades and currently executed in a PWR PACTEL configuration. This facility was built to investigate phenomena related to EPR-type reactors. Experiments have mostly focused on SB LOCA (Kouhia 2012).

Thus, using these codes in a body with experimental data cumulated during past decades has opened possibilities for researchers to reveal potential threads, support constructional aspects of new NPP, improve understanding of phenomena taking place during accidents on NPP.

1.2. Goals and structure of the thesis

To research natural circulation of LWRs and processes being involved in accidental situations such as SB LOCA, PACTEL facility was constructed at LUT and experiments were executed. The thesis is concentrated in modelling thermal hydraulics of PWR PACTEL facility in conditions of SB LOCA by using TRACE code. Obtained computed data needs to be analyzed and compared to experimental data.

2 PWR PACTEL FACILITY DESCRIPTION

2.1. General

The PWR PACTEL installation includes comprise of a reactor pressure vessel model, two loops with vertical steam generators, a pressurizer, and ECCS. The pressure vessel model of the facility, ECCSs, and pressurizer are taken from the original PACTEL facility. Consequently, those parts were designed with no reference to EPR details. The PWR PACTEL facility has absolutely new parts such as EPR style two vertical steam generators together with loops. The principal view of the PWR PACTEL facility is shown in Figure 1(Kouhia, Riikonen et al. 2014).

Since the PWR PACTEL is a modification of the PACTEL facility, the common parts such as the pressure vessel model, pressurizer, and ECCSs were maintained in the same manner as with the original PACTEL facility. Presence of newly designed loops along with vertical steam generators in the PWR PACTEL facility makes principal difference in comparison to the original construction. The VVER type NPP implementation of loop was modelled by the original PACTEL facility where each of three loops contained a horizontal steam generator, while as the PWR PACTEL facility included two loops with vertical generators. General characteristics of the PWR PACTEL facility are presented in Table 1(Kouhia, Riikonen et al. 2014).

The basic design principle of the PWR PACTEL involved using the greatest possible amount of parts of the original installation. Exclusively the new loops of primary coolant circuit and vertical steam generators were constructed ex novo in order to model EPR special aspects. The construction of the laboratory building imposed its constraints on possible design of height of vertical steam generators. The volumetric scaling was not preserved and the steam generators are shorter those utilized in EPR type NPP (Kouhia, Riikonen et al. 2014).

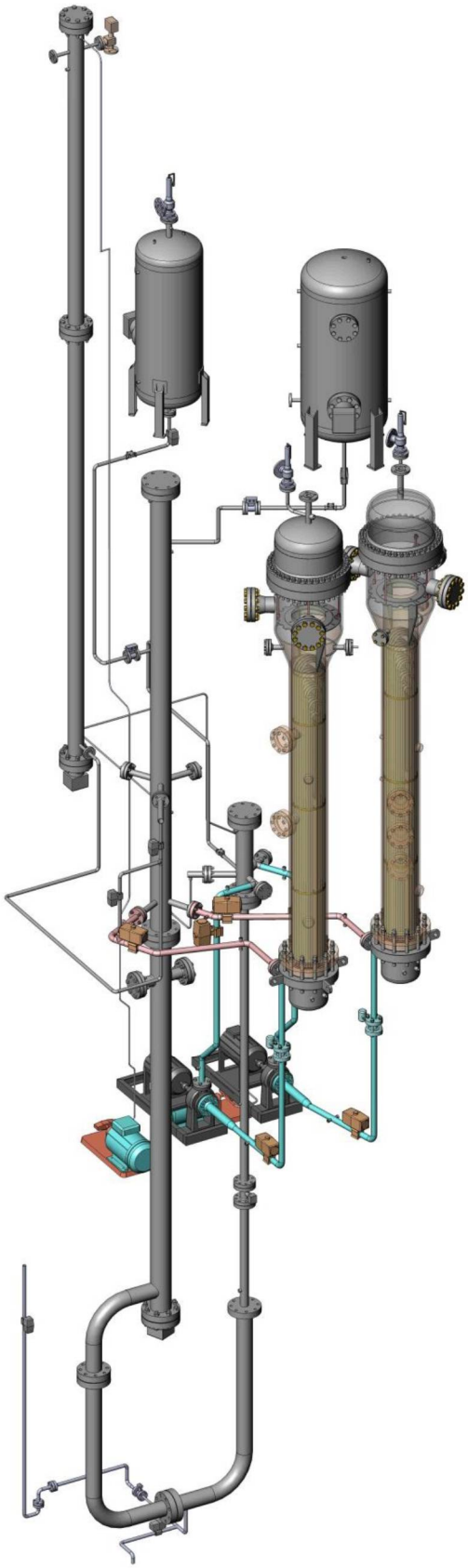

Figure 1: PWR PACTEL facility (Kouhia, Riikonen et al. 2014)

Table 1: PWR PACTEL facility characteristics

CHARACTERISTICS	***PWR PACTEL***
Reference power plant (loops and steam generators)	PWR (EPR)
Volumetric scale: pressure vessel, steam generators, pressurizer	1:405, 1:400, 1:562
Height scale: pressure vessel, steam generators, pressurizer	1:1, 1:4, 1:1.6
Number of primary loops	2
Maximum core heating power [MW]	1
Number of fuel rod simulators	144
Outer diameter of fuel rod simulators [mm]	9.1
Heating length of fuel rod simulators [m]	2.42
Axial power distribution of the core section	chopped cosine
Axial peaking factor of the core section	1.4
Maximum fuel rod simulator cladding temperature [ºC]	750
Maximum design primary / secondary pressure [MPa]	8.0 / 4.65
Maximum design primary / secondary temperature [ºC]	300 / 260
Steam generator heat exchange tube diameter / thickness [mm]	19.05 / 1.24
Average steam generator heat exchange tube length [m]	6.5
Number of heat exchange tubes in steam generator	51
Number of instrumented heat exchange tubes in SG1/ SG2	8 / 51 (14) a
Maximum secondary side feed water mass flow [l/min]	30
Maximum feed water tank pressure [MPa]	2.5
Maximum accumulator pressure [MPa]	5.5
Maximum HPIS/LPIS water pressure [MPa]	8.0 / 0.7
Main material of components	stainless steel (AISI 304)
Insulation material	mineral wool (aluminium cover)

2.1.1. Pressure vessel model and core components

The material from which the pressure vessel model is made of is stainless steel (AISI 304). The pressure vessel is intended for the pressure of 8 MPa and liquid temperature of 300 ºC. The construction has thermal insulating consisted of 100 mm thick layer of mineral wool covered by an aluminium plate with 0.7 mm thickness. Conceptual design of the pressure vessel model is shown in Figure 2 (Kouhia, Riikonen et al. 2014). The overall height of the pressure vessel model is compatible with the height of the pressure vessel of the EPR type NPP. The volume ratio between the reactor pressure vessel of EPR plant and the modelled PWR PACTEL pressure vessel is 1/405 (Kouhia, Riikonen et al. 2014).

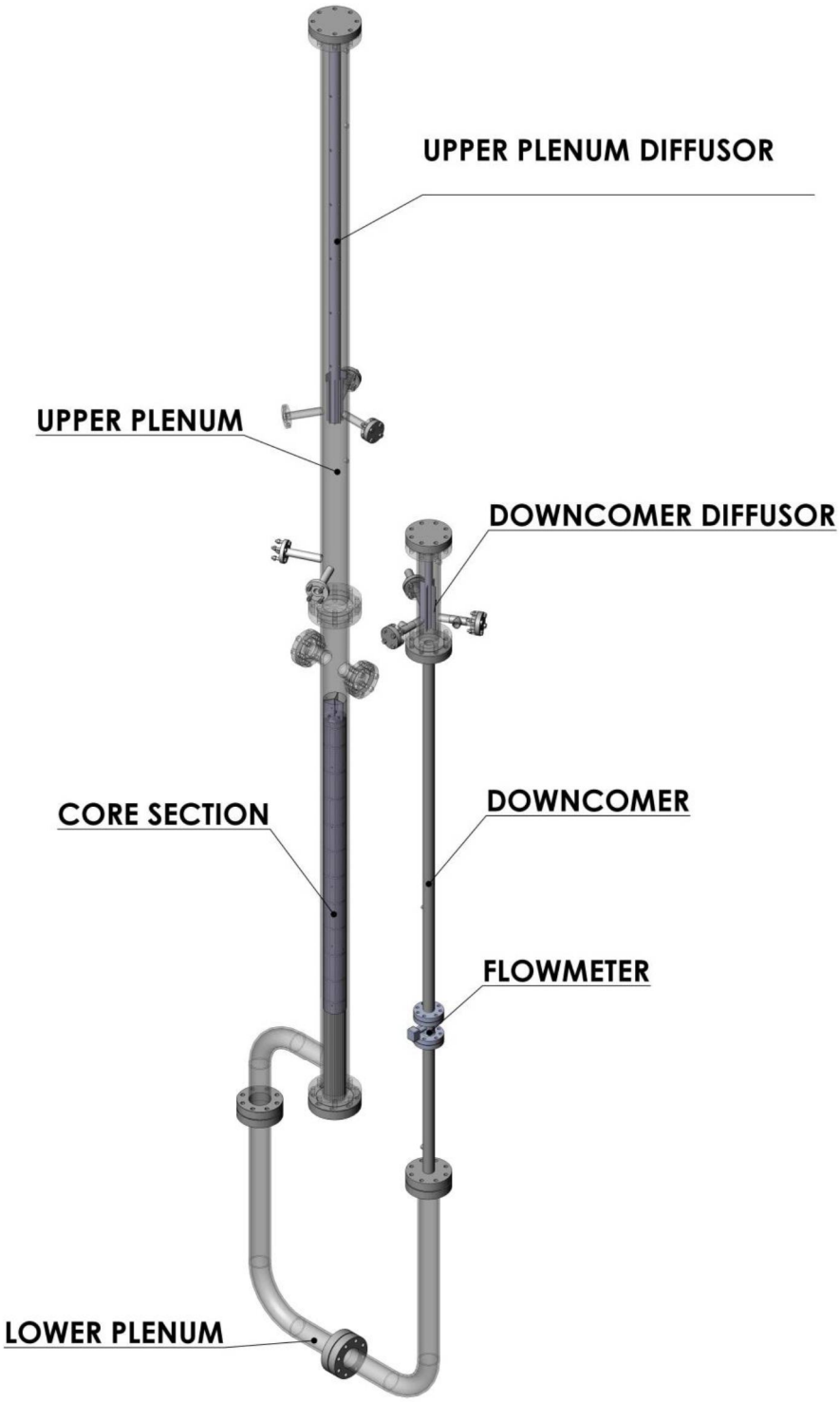

Figure 2: Pressure vessel model of PWR PACTEL (Kouhia, Riikonen et al. 2014)

2.1.1.1. Core

The configuration of the PWR PACTEL core remained unchanged from the original PACTEL facility and shown in Figure 3. The core comprises 144 heating elements forming the rod bundle. These elements simulate fuel rods (further ”rods”) heated electrically. Dimensional characteristics of the rods are: 9.1 mm is the outer diameter and 0.9 mm is the thickness of cladding made from stainless steel (AISI 316L). The layout of rods has triangular shape with lattice pitch of 12.2 mm. The axial peak factor equals 1.4 and the total heating length is 2420 mm. In between stainless steel cladding and the heating inductor magnesium oxide insulation is placed. The rods are fitted with the thermocouples attached to the cladding surface. The rods are separated in three parts of 48 in each part within specific shroud. The construction completed with 12 spacer grids and 30 support rods installed inside the bundle. The rod bundle is fitted with a special choke plate on the upper part. The greatest possible value of the core power is 1 MW. All three channels are able to be maintained with different power levels. Figure 3 (Kouhia, Riikonen et al. 2014) illustrates the construction of the core.

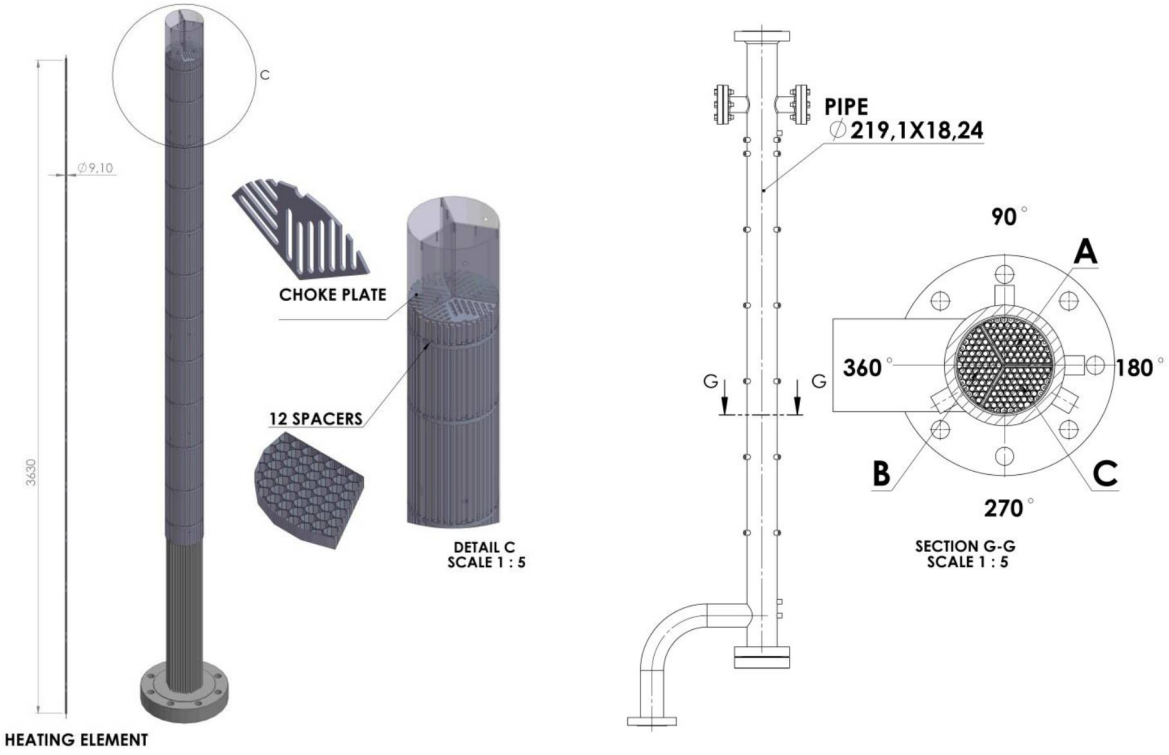

Figure 3: The core construction (Kouhia, Riikonen et al. 2014)

The heating length of the bundle is two meters shorter than the heating length of EPR core, though elevation of the core's center is on the corresponding point. The highest core power covers the scaled residual heating power of EPR type reactor (Kouhia, Riikonen et al. 2014).

2.1.1.2. Upper plenum, downcomer, and lower plenum

Whereas, in the PWR PACTEL facility major components are used from the original PACTEL facility construction, some components have undergone changes. Thus, for connection of two new vertical steam generators the upper plenum configuration needed to be changed. The new hot leg connection elevation is lower than the connection of the original facility. The height of the upper plenum is 5 m long. Inside the upper plenum in the top part there is a diffuser 3.6 m long. The upper plenum and the downcomer do not have any by-pass connections. The excess of the maximum credible value of pressure of the whole facility can be prevented by a safety valve located on the top of the upper plenum.(Kouhia, Riikonen et al. 2014)

The lower plenum presents as U-shape construction consisting of two parts similar diameter. In its turn, the downcomer consists of upper and lower parts. The first part is 0.9 m long and has a bigger diameter by comparison with lower part. The smaller diameter of the lower part is attributable to connection to the cold leg. The downcomer is equipped with 0.8 m long diffuser which is installed in the top part of the downcomer. The purpose of presence of both diffusors in the upper plenum and the downcomer is to avoid the direct flow of water from ECCS to the loops of the original PACTEL facility.(Kouhia, Riikonen et al. 2014)

2.1.2. Primary loops

The PWR PACTEL facility is simulating the EPR type NPP, thus the presence of two new vertical steam generators implicates creating new primary loops. Inasmuch as the EPR has four primary loops, the PWR PACTEL facility is simulating the half of EPR capacity. The loops are covered with insulation of 60 mm thick layer of mineral wool and 0.7 mm thick aluminium plate. The inside diameter of both cold and hot legs is 52.5 mm. Both cold legs are equipped with main circulating pumps. The pressurizer is connected with the hot leg of Loop

2. Each leg is equipped with the isolating valve in order to have opportunity to isolate a loop if required(Kouhia, Riikonen et al. 2014).

2.1.3. Main circulation pumps

Initially, the PWR PACTEL was not equipped with the main circulation pumps. The facility was modified in 2013. Table 2 (Kouhia, Riikonen et al. 2014) provides basic characteristics of the main circulation pumps.

Table 2: Characteristics of the main circulation pumps

CHARACTERISTICS	***VALUE***
Manufacturer	KSB
Type	Centrifugal pump, KSB HPH 50-200
Operating head [m]	19.20
Operating flow [m3/h]	25.00
Nominal speed [rpm]	1440
Operating efficiency [%]	65.0
Density [kg/m3]	799.2
Pump power at Tact / power at T0° / motor power [kW]	1.8 / 2.2 / 3

2.1.4. Steam generators

Newly created vertical steam generators had the purpose to model EPR type stem generator's behavior. The accuracy of scaling principles was not fully accomplished because of the laboratory building imposed restrictions. Nevertheless the height of steam generators equals to a fourth of EPR type steam generators. Accordingly, volumetric scaling was not preserved. The general view of the steam generators is shown in Figure 4 (Kouhia, Riikonen et al. 2014).

One vertical steam generator comprises 51 heat transfer U-shape tubes presented in Figure 5 (Kouhia, Riikonen et al. 2014). The heat transfer tubes with inner diameter 19.05 mm and wall thickness of 1.24 mm have average length of 6.5 m and complete with triangular grid. The lattice pitch is 27.4 mm. The tubes split into five groups. Each group has different length of the tubes. The total heat exchange area of the tubes and the volume of the primary coolant system

of each steam generator resolve itself to 1/400. The bottom of each steam generator has two cold and hot plenums confined from the top with tube sheet.

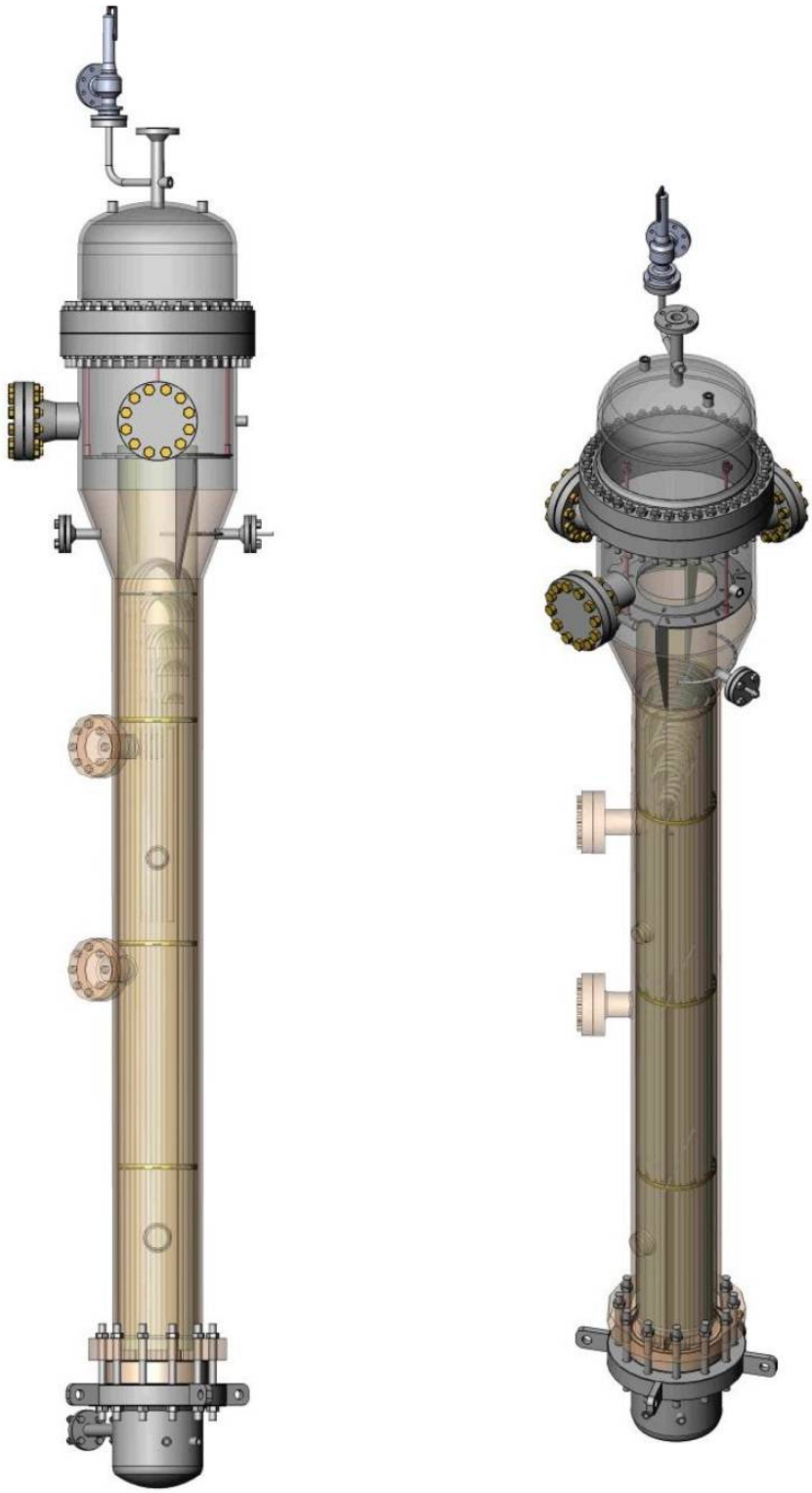

Figure 4: General view of the PWR PACTEL steam generator (Kouhia, Riikonen et al. 2014)

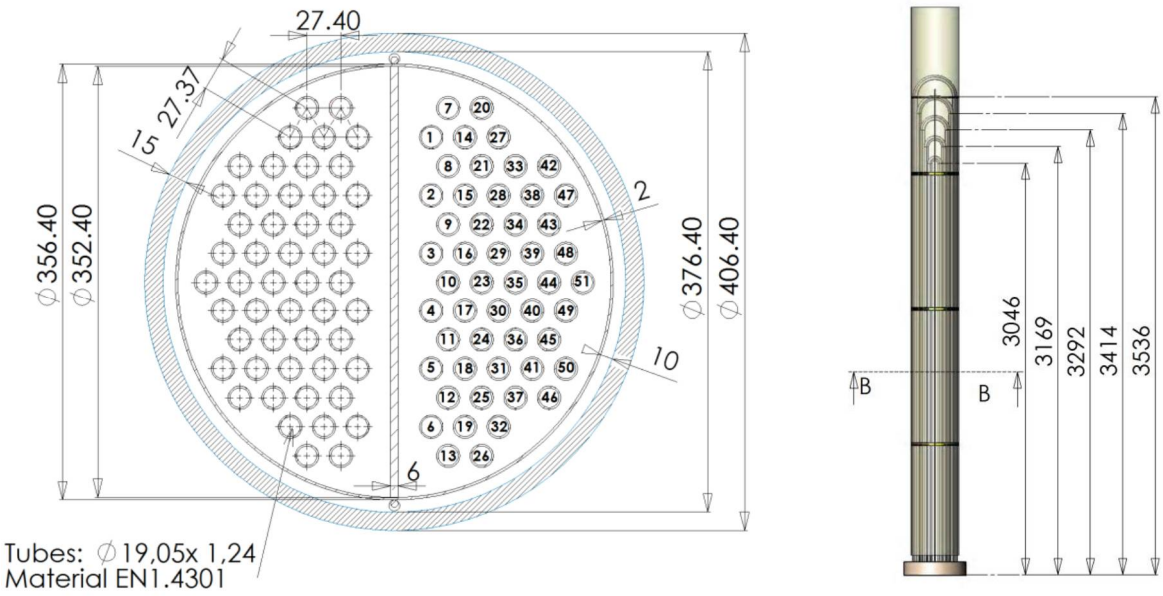

Figure 5: Heat transfer tubes of the PWR PACTEL steam generators (Kouhia, Riikonen et al. 2014)

Volumetrically the secondary system of the vertical steam generator is divided in several parts. The bottom part of the steam generator comprises the downcomer together with riser volumes. The heat transfer surface of the tube bundle is placed inside riser volume which in its turn surrounded by annular downcomer. The downcomer is separated in two hot and cold enclosures. The underpart of the riser is divided into hot and cold enclosures with divide wall as well. The enclosures have leakiness of water to each other from behind of manufacturing reasons. Thus, inconspicuous flows are possible between the cold and hot parts. The head of the steam generator is occupied by steam volume. There is a special plate which divides steam volume from the water volume. The condensed on the plate water flows to the hot side of downcomer (Kouhia, Riikonen et al. 2014).

The feed water injection is incorporated in the secondary side of both steam generators independently. The feed water injection system is installed in the cold upper part of the downcomer. The steam generators have their own steam lines, which incorporate in one in order to eject secondary side steam to the atmosphere. Each steam line has a set of safety and control valves (Kouhia, Riikonen et al. 2014).

The secondary side volume is in excess because of small steam generator scale. From volumetric scaled volume point of view the volume of PWR PACTEL steam generators is doubled in comparison with the EPR steam generators. The PWR PACTEL steam generators do not include the modelling of steam separators. The steam generators are covered by 100 mm thick mineral wool insulation and an aluminium coat of 0.7mm thick (Kouhia, Riikonen et al. 2014).

2.1.5. Pressurizer

The construction of the pressurizer of PWR PACTEL facility is identical to the original PACTEL facility. The pressurizer is cylindrical pressure vessel consisting of two parts with the same inside diameter of 139.7 mm. The parts are jointed with flanges. The clearance height of the pressurizer is 8.8 m. The pressurizer is connected to the hot leg of Loop 2. The pressurizer surge line has length of 7.8 m with inner diameter of 27.3 mm. The pressure of the primary circuit is maintained by heating and spray systems of the pressurizer. The heating system consists of three heaters with power of 2, 4 and 7 kW. For safety purposes a relief valve is located on the top of the pressurizer. The pressurizer is covered by insulation as the steam generators with 100 mm thick mineral wool and an aluminium plate cover of 0.7 mm. The pressurizer surge line has less thickness of mineral wool (35 mm) (Kouhia, Riikonen et al. 2014).

The pressurizer in the same manner as the steam generators, because of the laboratory building physical constraints is shorter than the EPR type pressurizer. The volume difference between the pressurizer of the PWR PACTEL facility and the pressuriser of the EPR type NPP is 1/562 (Kouhia, Riikonen et al. 2014).

2.1.6. Emergency core cooling systems

The ECCSs of the original PACTEL facility remained unchanged for the PWR PACTEL facility. These systems consist of the low pressure injection system (LPIS) and the high pressure injection system (HPIS). Two separate accumulators together with a low pressure injection pump assemble the LPIS. The first accumulator has volume of $1m^3$. The injection pipeline is jointed to the upper plenum. The second accumulator is less than the first one and its volume

equals 0.6 m^3. The injection pipeline is jointed to the downcomer. The HPIS has two possible ways of utilization for PWR PACTEL facility, either via the cold leg connection of the original PACTEL facility or there is a new connection can be installed later. General characteristics of the ECCSs are shown in the Table 3 (Kouhia, Riikonen et al. 2014).

Table 3: Characteristics of the ECCSs

CHARACTERISTICS	***VALUE***
Accumulators, maximum pressure [MPa]	5.5
LPIS, maximum pressure [MPa]	0.7
HPIS, maximum pressure [MPa]	8.0
Feed water tank, pressure [MPa]	2.5
Feed water tank, maximum temperature [ºC]	225

2.1.7. Water treatment and start up procedures

The actuation fluid for both primary and secondary side is the water out of a tap. Before the injection the water is undergoes procedures of the demineralizing, softening and mixing with some alkaline boiler water. Deaerating of the water was not carried out in all PWR PACTEL facility experiments.

There are two basic steps in the PWR PACTEL facility start-up procedure. Firstly, the facility is filled in with the water and heated up during 4-5 hours. Secondly, the stabilization phase is taking place for 1-2 hours in average. During the start-up period, noncondensable gases are released out of the water venting of the facility from the upper parts of the primary circuit (Kouhia, Riikonen et al. 2014).

2.2.Design and scaling principles

2.2.1. Design principles

The PWR PACTEL facility was created in order to explore unique EPR accident management procedures and collect invaluable experience of the EPR type PWR behavior. The primary focus of the study was on the vertical steam generators and their primary loop behavior. Both the new vertical steam generators and corresponding loops are created in a manner to simulate, as

great as practicable EPR type facility, in order to achieve objective simulation of EPR peculiarities (Kouhia, Riikonen et al. 2014).

Such parts as the pressure vessel model, pressurizer and ECCSs are common for both the original PACTEL facility and the PWR PACTEL facility, which is an important aspect. By doing this, there is possibility to use the original PACTEL facility in cases of necessity is preserved. The basic layout of both facilities in the laboratory building is shown in Figure 6 (Kouhia, Riikonen et al. 2014).

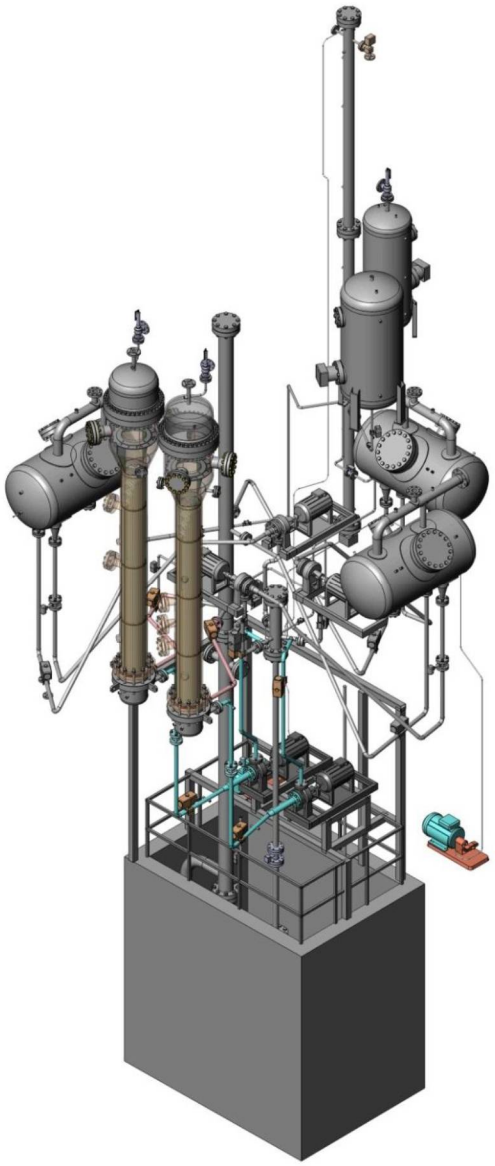

Figure 6: PACTEL and PWR PACTEL facilities basic layout in the laboratory building (Kouhia, Riikonen et al. 2014)

2.2.2. Scaling approach

With the object to make possible the simulation of EPR peculiarities, the new vertical steam generators along with loops were particularly designed. Owing to external restrictions such as the construction of the laboratory building, the scaling accuracy was not entirely accomplished. Despite that the height of new steam generators was maximized they cover only one fourth of the height of the EPR type steam generator. Thus, from volumetric scaling point of view there is some inaccuracy exists. Because of the limitations imposed by the laboratory building on the scaling accuracy approach, volumetric scaling compromise needs to be found on an equal basis with the height of the steam generators. However, it is recognized that for net impression of the basic phenomena attributed to the vertical steam generator performance in operational and accidental situations, the accuracy of the PWR PACTEL facility is high enough. The arrangement of the facility within the laboratory building is shown in Figure 7 (Kouhia, Riikonen et al. 2014).

The inside diameter of heat exchange tubes of the steam generator in the PWR PACTEL facility is absolutely identical to EPR type steam generator. The fulfilment of such condition is important for proper simulation of counter-current flow limitation (CCFL) phenomena. Considering that the secondary side volume of the EPR steam generators is twice as much as the volume of the PWR PACTEL steam generator secondary side, it causes an excess of water mass in the PWR PACTEL secondary side (Kouhia, Riikonen et al. 2014).

One of the EPR type plant loops is simulated by the one and the other primary coolant loops of the PWR PACTEL. The main designing approach of pipe dimensions in PWR PACTEL facility of cold and hot legs ensues to Froude scaling, along with volumetric scaling principles. In such a manner, the flow regime transitions simulation of horizontal parts of the loops is achieved better values. The pressure loss distribution longwise the loop is changed because of the usage of volumetric scaling (Kouhia, Riikonen et al. 2014).

By applying the volumetric scaling approach, the reduction of the volumes and flow areas of the loops occurs. Generally, the overestimation of the thermal losses to the environment happens via use of the volumetric scaling. Over the matter of that the ratio of the surface tube area

to the volume of the tube is higher for the scaled down facility rather than for the original facility. Similarly, an unduly high ratio of the wall mass to the volume of water is caused by the volumetric scaling principle. The qualitative insulation is envisaged in all PWR PACTEL facility elements in order to avoid additional thermal losses. The absolute value of the thermal losses essentially depends on the temperature of the primary loop (Kouhia, Riikonen et al. 2014).

The opted scale of the pressurizer has an effect on the distribution of the void fraction in blowdown situations. The distribution of the void fraction of the EPR pressurizer is not uniform, whereas the scaled down pressurizer has the uniform distribution. This is a significant aspect in cases of some transients, as a large mass of water may be accumulated in the pressurizer and not be available in the core cooling system (Kouhia, Riikonen et al. 2014).

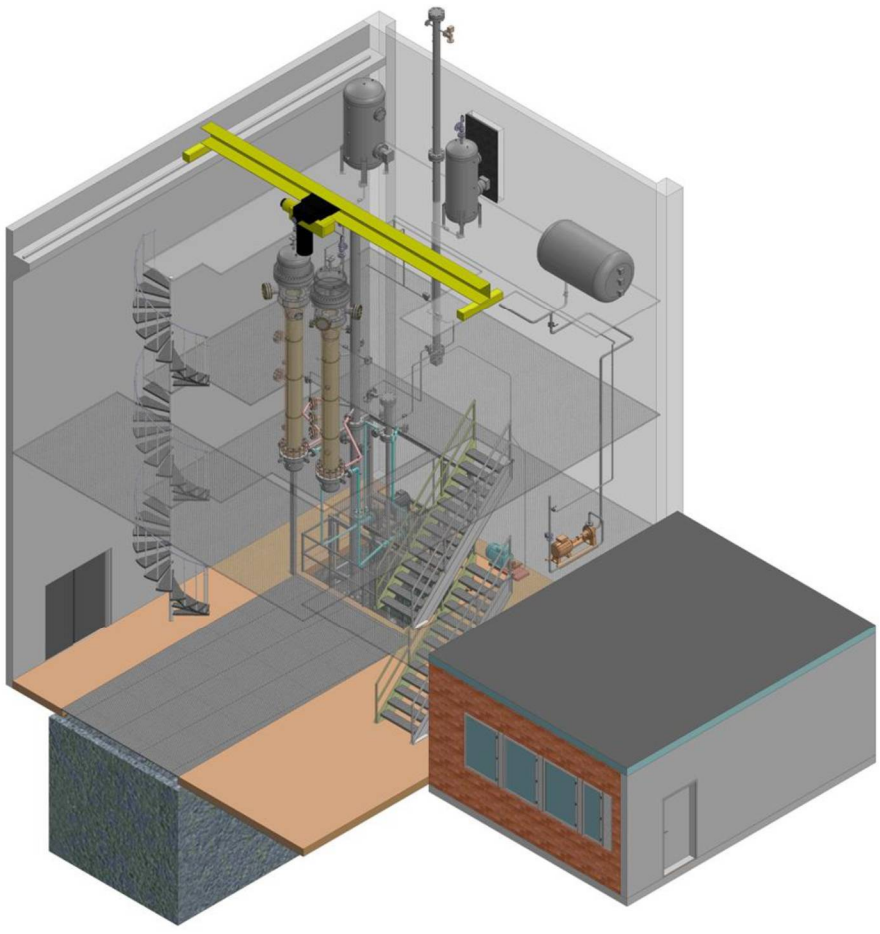

Figure 7: The PWR PACTEL facility arrangement inside the laboratory building (Kouhia, Riikonen et al. 2014)

2.3.Instrumentation

There are three types of instrumentation equipment the facility has. It is temperature pick-ups, pressure-measuring devices, and flowmeters. Together with them, the core power, the pressurizer heaters power, and main circulation pumps power are under control (Kouhia, Riikonen et al. 2014).

2.3.1. Temperature acquisitions

Three basic types of temperature are measured, such as coolant temperature, cladding of the rods temperature, and air in laboratory building. The greater part of temperature gauges of the facility is K-type (NiCr-Ni; wall AISI316L) thermocouples with mineral insulation. The fraction of the temperature measurements was made by resistance detectors (RDT) of platinum type (PT-100) along with negative temperature coefficient (NTC) thermistors. All temperature detectors are unearthed. The outside diameter of the temperature detectors, depending on the measurement point, changes from 0.5 mm to 6 mm (Kouhia, Riikonen et al. 2014).

All the temperature-sensing devices are connected with the modules of National Instruments Compact FieldPoint (Ni cFP) data acquisition system (cFP-1808). The cFP modules possess a cold junction temperature compensation system, which allows determining the correct temperature for all channels of temperature acquisition. In order to cut to a minimum the internal heating of the RTDs, there is impulse excitation current is used in the RTD modules (Kouhia, Riikonen et al. 2014).

2.3.1.1. Core

Both, the rod cladding temperature and fluid temperature in the core section are measured with thermocouples. The outer diameter of thermocouples is 0.5 mm. The thermocouples liable for the cladding temperature measurements are attached to outside surface of the rod cladding by TIG welding. The measurements of fluid temperature inside the rod bundle are implemented in such a manner that the thermocouple measurement point is distant from the outer surface of

the rod. The distribution of thermocouples within the core section is shown in the Table 4 (Kouhia, Riikonen et al. 2014).

Table 4: Thermocouples in the rod bundle of the core section.

Measurement	***Number of measurement points***
Cladding temperature, channel A	24
Cladding temperature, channel B	24
Cladding temperature, channel C	23
Fluid temperature, channel A	5
Fluid temperature, channel B	5
Fluid temperature, channel C	5
Total	*86*

2.3.1.2. Steam generators

Steam generator 1 comprises eight thermal exchange tubes, which are instrumented. The primary circuit fluid temperature in those tubes is measured with thermocouples of 1.5 mm in four different points. The technical performance of the thermocouples is shown in Figure 8 (Kouhia, Riikonen et al. 2014). The instrumentation of the second steam generator is more intensive. Each heat exchange tube of this steam generator has at least one measurement point. Nine out of fifty one tubes have eight points to measure the fluid temperature and four tubes fitted with six measurement points in each tube. The only tube in the second steam generator has 13 points for fluid temperature measurements. All the other tubes of the second steam generator have only one measurement point in the bottom part of the cold side (Kouhia, Riikonen et al. 2014).

The measurements of the secondary side fluid temperature were implemented by 14 thermocouples in each steam generator. Riser volume of each steam generator contains nine thermocouples, steam volume has two and three belong to downcomer volumes. The outer diameter of the thermocouples belonging to riser and steam volumes is 1.5 mm. The technical performance of the thermocouple joint in the riser volumes is shown in Figure 9 (Kouhia, Riikonen et al. 2014). The rest of the thermocouples have 3 mm diameter (Kouhia, Riikonen et al. 2014).

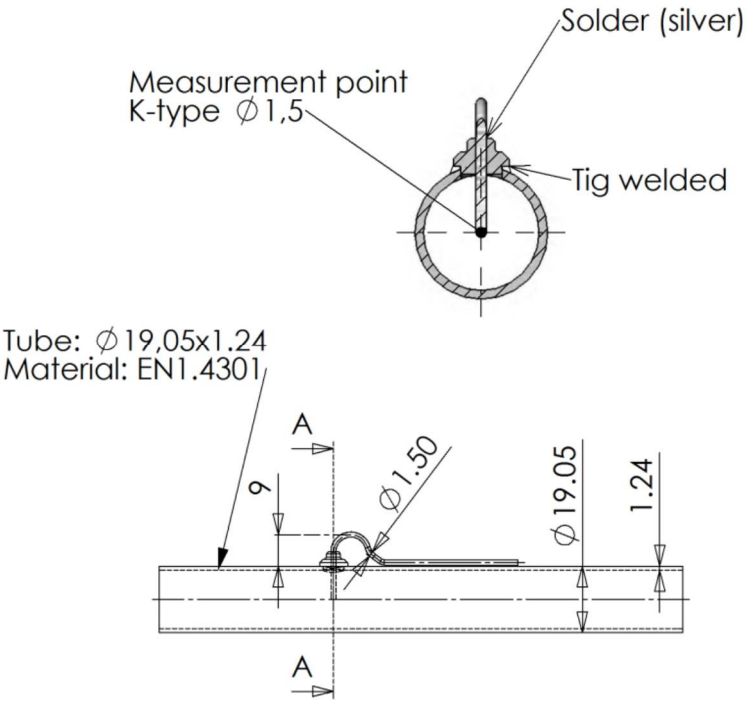

Figure 8: Technical performance of thermocouple joint for steam generator heat exchange tubes on the primary side (Kouhia, Riikonen et al. 2014)

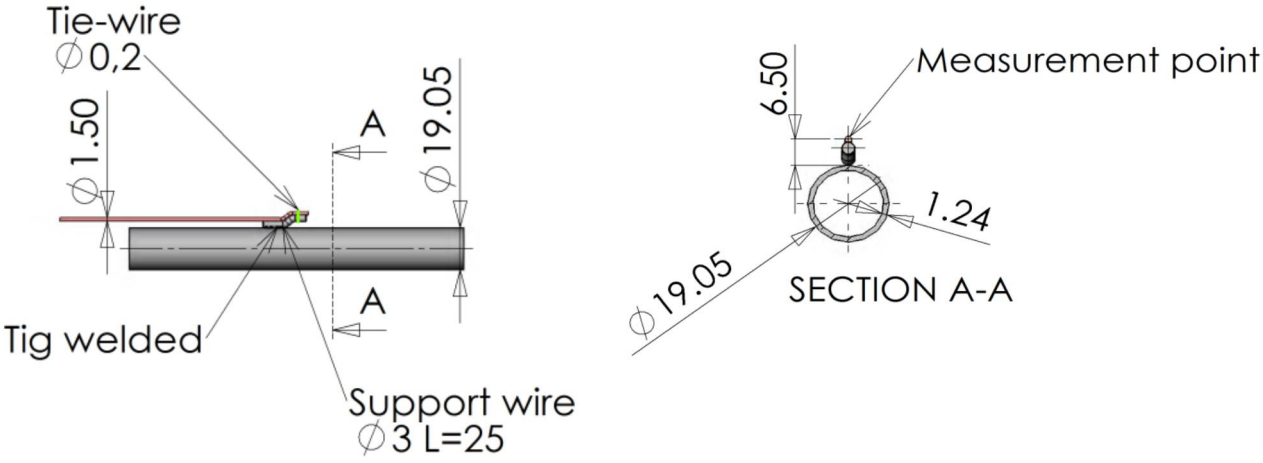

Figure 9: Temperature measurement method for the steam generator secondary side in the heat exchange tube area (outside the tube) (Kouhia, Riikonen et al. 2014)

2.3.1.3. Other temperature acquisitions

The rest fluid temperature measurement points along the facility such as primary loops and other not mentioned locations were implemented with 3 or 6 mm thermocouples or with RTDs. The air temperature in the laboratory building is measured at seven elevations. There

are also some measurements of structure temperature envisaged. (Kouhia, Riikonen et al. 2014)

2.3.2. Pressure measurements

Variety of pressure sensing probes is used in the PWR PACTEL facility. These instrumentalities serve to measure the pressure at the top of the upper plenum and pressurizer, and the secondary system of the steam generators. The pressure measurements is also afforded in the ECCS accumulators (Kouhia, Riikonen et al. 2014)

2.3.3. Differential pressure measurements

A number of pressure-difference transmitters are installed in the PWR PACTEL facility in order to estimate the collapsed level. Differential pressure transducers are installed in six thermal exchange tubes of the steam generator 2 (Kouhia, Riikonen et al. 2014).

2.3.4. Flow rate meters

Both cold legs and the downcomer are complete with flowmeters. The LPIS has three flowmeters. The first flowmeter is installed in the accumulator 1 line and the LPIS pump connection. The second flowmeter measures flow in the line between the accumulator 2 and the LPIS pump connection. The last out of those three flowmeters is installed in the LPIS pump line. The HPI system has the only flow meter. Complementarily, secondary side feed water lines of both steam generators have a flow meter each. The pressurizer spray line is equipped with its own flow meter as well (Kouhia, Riikonen et al. 2014).

2.3.5. Core heating power

Each core rod bundle section is individually supplied with power by AEG Thyrobox. The NORMA D5255S Power Analyser determines the output power. The determined energy consumption within the experiments allows the measurement of the average core power (Kouhia, Riikonen et al. 2014).

3 TRACE CODE OVERVIEW

Current chapter is dedicated to overview of basic principles of the TRACE code used over the modelling of the facility mentioned in the preceding chapter. The overview includes such aspects as TRACE code characteristics, list of physical phenomena considered, limitations on use, field equations.

During last years, different countries have been working on elaboration of advanced computational tools in the matter of simulating reactor facility behavior within transient processes either real or hypothetical. Thus, obtained experience of using such tools can make a tremendous contribution to design, operation and safety aspects of NPP.

One of the latest in a series of advanced reactor systems codes is TRACE. The code was developed by the U.S. Nuclear Regulatory Commission and allows analyzing of transient and steady-state neutronic-thermal-hydraulic behavior of LWR. The main purpose of developing TRACE is the ability to provide the estimations of LOCAs, operational transients and other accidental situations in LWR. The code is also applicable for modelling processes occurring in experimental facilities dedicated to simulate transients of reactor systems.

The finite volume approach is used in order to solve the partial differential equations describing two-phase flow along with heat transfer processes. From the spatial point of view the fluid-dynamics equations are one-dimensional. There are also three-dimensional components in use (U. S. NRC 2007).

The TRACE code is based on a component modeling of a reactor system. Each physical part of the equipment in a flow loop can be presented as a component. All of the components can be nodalized in any number of physical volumes, which are also called cells. There is no limitation on either number of components used in the system simulation or the way of their coupling together. The list of reactor hydraulic components comprise PIPEs, PLENUMs, PRIZERs (pressurizers), CHANs (BWR fuel channels), PUMPs, JETPs (jet pumps), SEPDs (separators), TEEs, TURBs (turbines), HEATRs (feedwater heaters), CONTANs (containment), VALVEs, and VESSELs (with associated internals) (U. S. NRC 2007).

3.1. TRACE Characteristics

A flow calculation for reactor components where three-dimensional phenomena occur can be simulated with 3D (x, y, z) Cartesian- and/or (r, θ, z) cylindrical-geometry approach. Such components, with 3D flow phenomena simulating, are called VESSELs. The compatibility of one- and three-dimensional components achieves precise modeling of intricate systems together with local multidimensional flows. These options are highly important in cases of ECCSs modeling during LOCA (U. S. NRC 2007).

The code is able to work with non-homogeneous, non-equilibrium modeling approach. A two-phase flow is delineated with six-equation hydrodynamic model. Such model allows simulating counter current flow phenomena explicitly (U. S. NRC 2007).

The whole thermal-hydraulics equation combination describes the mass, momentum and energy transfer between phases of the two phase flow as well as the interference of a heat flow with the phases. Inasmuch as the flow topology imposes constraints on this interference, thus a flow-regime dependent constitutive-equation package was fitted into the TRACE code (U. S. NRC 2007).

TRACE possesses the wide range of applicability. The amount of components provided by the code is enough for modelling of any LWR experimental configuration.

3.2. Physical phenomena considered

The TRACE code is able to simulate phenomena peculiar to either large-break or small-break LOCA analyses such as:

1) ECC downcomer penetration and bypass, including the effects of countercurrent flow and hot walls;
2) Lower-plenum refill with entrainment and phase-separation effects;
3) Bottom-reflood and falling-film quench fronts;
4) Multidimensional flow patterns in the reactor-core and plenum regions;

5) Pool formation and countercurrent flow at the upper-core support-plate (UCSP) region;
6) Pool formation in the upper plenum;
7) Steam binding;
8) Water level tracking;
9) Average-rod and hot-rod cladding-temperature histories;
10) Alternate ECC injection systems, including hot-leg and upper-head injection;
11) Direct injection of subcooled ECC water, without artificial mixing zones;
12) Critical flow (choking);
13) Liquid carryover during reflood;
14) Metal-water reaction;
15) Water-hammer pack and stretch effects;
16) Wall friction losses;
17) Horizontally stratified flow, including reflux cooling,
18) Gas or liquid separator modeling;
19) Noncondensable-gas effects on evaporation and condensation;
20) Dissolved-solute tracking in liquid flow;
21) Reactivity-feedback effects on reactor-core power kinetics;
22) Two-phase bottom side, and top offtake flow of a tee side channel; and reversible and irreversible form-loss flow effects on the pressure distribution (U. S. NRC 2007)

3.3.Limitations on use

The TRACE code has series of limitations on application which needs to be taken into account. TRACE was basically developed for investigation of large and small break LOCA in such type reactors as the Economic Simplified Boiling Water Reactor (ESBWR) along with PWR and BWR apart of B&W design. However, it is worth to mention that assessment of BWR processes by using the TRACE code is less intense in comparison to PWR (U. S. NRC 2007).

The calculations where flow momentum transfer needs to be considered in a more precise manner at a local level cannot be done by using TRACE. The shape of the velocity cross pro-

file has significant importance. In those elements where the profile is not flat the fluid dynamics will not be captured in detail (U. S. NRC 2007).

The code is very exacting to the reactor core power distribution. The exceedance of power on local level, which causes significant asymmetries in power profile, such as can happen during control rod ejections, can be calculated using additional modules, like PARCS spatial kinetics module (U. S. NRC 2007).

TRACE has its own limitations on use in cases where viscous stresses of the same magnitude or perceptibly higher with the wall or interfacial shear stresses. The reason of that is in the code field equations, during derivation of which the shear stresses were negligible (U. S. NRC 2007).

Thermal stress estimations of a facility structure do not belong to TRACE competence. There is no explicit modeling method of such effects as material thermal expansion owing to which the fuel rod gas gap closure occurs. More detailed analysis programs can be supported by TRACE code (U. S. NRC 2007).

Whereas the TRACE code possesses approximations in terms of wall and interface heat flux it can cause inaccuracy of estimations such phenomena as collapse of a steam bubble, which is vital for B&W candy-cane natural circulation calculations (U. S. NRC 2007).

3.4.Field Equations

The field equation set utilized in modeling of two-phase flow was derived from Navier-Stokes equations for both phases. The set of field equations comprises of distinct mass, momentum, and energy conservations for both gas and liquid phases. All of the used equations are subject to time averaging. Such model was stated as formally ill-posed, which caused plenty debates (Bruce Stewart, Burton 1984). However, the numerical solution in the aggregate with minor enhancements within the field equation set shows that the model can be considered as relatively well-posed, which was fortified by Stewart (Bruce Stewart 1979).

As it was mentioned before, the field equations set consists of three types of equations, that are mass, momentum, and energy conservation equations. In cases of two-phase flow it means that basis of the model has six partial differential equations (PDEs) allowing to describe steam/water flow. During LOCA, noncondensable gases such as nitrogen from accumulators and air of containment building can possibly permeate into the system. That would lead to mixing steam phase with those gases which needs to be considered. There are several assumptions are made in the TRACE code. First, the velocities of the mixture components are the same. Second, the temperatures of those components are the same as well. Ultimately, the momentum and energy conservation equation do not distinguish within the mixture. However, in case of mass conservation equation, additional equation is required in order to estimate relative concentration of noncondensable gases inside steam phase. Nitrogen from accumulators and air are coupled together under noncondensable gases term because of similarity of their properties. Thus, the set of PDEs being complemented with one more mass equation. Nevertheless, in case of need, the distinction within noncondensable gases can be easily accomplished (U. S. NRC 2007).

By nearly the same principle as with noncondensable gases, the boron concentration tracking can be implemented. An additional mass concentration equation completes the set of PDEs. An assumption needs to be made that fraction of boric acid is next to negligible for having influence on the liquid. Thus, the liquid momentum equation stays unchanged (U. S. NRC 2007).

The summarized field equations set is shown below in Eqs (1) through (6). Both single phase gas and single phase liquid conservation equations are time averaged. Interface jump conditions are included in the equations set derivations. The following terms represent: α is the probability of point in space being occupied by gas; Γ, E_i, M_i are the terms responsible for interface jump conditions in mass, energy and momentum conservation equations respectively. The conductive heat flux is denoted with q'. q_d belongs to direct heating in terms of radioactive decay. (U. S. NRC 2007).

Time Averaged Mass Equations

$$\frac{\partial[(1-\alpha)\bar{\rho}_l]}{\partial t} + \nabla \cdot \left[(1-\alpha)\bar{\rho}_l \bar{\vec{V}}_l\right] = -\bar{\Gamma} \tag{1}$$

$$\frac{\partial[\alpha\bar{\rho}_g]}{\partial t} + \nabla \cdot \left[\alpha\bar{\rho}_g \bar{\vec{V}}_g\right] = \bar{\Gamma} \tag{2}$$

Time Averaged Energy Equations

$$\frac{\partial\left[(1-\alpha)\bar{\rho}_l\left(\overline{e_l + \frac{V_l^2}{2}}\right)\right]}{\partial t} + \nabla \cdot \left[(1-\alpha)\bar{\rho}_l \overline{\left(e_l + \frac{V_l^2}{2}\right)\vec{V}_l}\right] = \\ = -\nabla \cdot \left[(1-\alpha)\overline{\vec{q}_l'}\right] + \nabla \cdot \left[(1-\alpha)\left(\overline{\mathrm{T}_l \vec{V}_l}\right)\right] + (1-\alpha)\bar{\rho}_l \overline{\vec{g} \cdot \vec{V}_l} - \bar{E}_\iota + \overline{q_{dl}} \tag{3}$$

$$\frac{\partial\left[\alpha\overline{\rho_g}\left(\overline{e_g + \frac{V_g^2}{2}}\right)\right]}{\partial t} + \nabla \cdot \left[\alpha\overline{\rho_g}\overline{\left(e_g + \frac{V_g^2}{2}\right)\vec{V}_g}\right] = \\ = -\nabla \cdot \left[\alpha\overline{\vec{q}_g'}\right] + \nabla \cdot \left[\alpha\left(\overline{\mathrm{T}_g \vec{V}_g}\right)\right] + \alpha\overline{\rho_g}\overline{\vec{g} \cdot \vec{V}_g} + \bar{E}_\iota + \overline{q_{dg}} \tag{4}$$

Time Averaged Momentum Equations

$$\frac{\partial\left[(1-\alpha)\bar{\rho}_l \bar{\vec{V}}_l\right]}{\partial t} + \nabla \cdot (1-\alpha)\bar{\rho}_l \overline{\vec{V}_l \vec{V}_l} = \nabla \cdot [(1-\alpha)\bar{\mathrm{T}}_l] + (1-\alpha)\bar{\rho}_l \vec{g} - \overline{M_\iota} \tag{5}$$

$$\frac{\partial\left[\alpha\overline{\rho_g}\bar{\vec{V}}_g\right]}{\partial t} + \nabla \cdot \alpha\overline{\rho_g}\overline{\vec{V}_g \vec{V}_g} = \nabla \cdot \left[\alpha\bar{\mathrm{T}}_g\right] + \alpha\overline{\rho_g}\vec{g} + \overline{M_\iota} \tag{6}$$

After sequence of transfigurations related to revision of time averaged field equations and their further volume averaging, a set of important approximations needs to be done:

1) The product of volume averages supposes to be the same as the volume average of a product.
2) The heat flux model has a partial lattice, which means that there is no heat conduction in the fluid between averaging volumes. This assumption does not allow to make pre-

cise calculations of the collapse of a steam bubble blocking natural circulation through a B&W candy cane, which makes TRACE is not applicable for this type of reactors.

3) The absence of shear forces in between adjoining averaging volumes. Only the sear at the metal surface and phase interfaces inside one volume are considered.
4) The ignorance of viscous heat transfer excluded pump components (U. S. NRC 2007).

Henceforth, variables included in following equations are considered to be time and volume averaged. The α is no longer a probability of a space point belonging to gas, but the fraction of the averaging volume being occupied by gas or simply void fraction. Such terms as q_{il} and q_{ig} are responsible for heat transfer from interface to liquid and to gas respectively. The heat transferred from surface of structures to the fluid is expressed through the following variables as q_{wl}, and q_{wg}. Thus, energy equations will take the form shown below: (U. S. NRC 2007).

$$-\overline{\nabla \cdot \left[(1-\alpha)\overrightarrow{q_l'}\right]} \Rightarrow q_{il} + q_{wl} \tag{7}$$

$$-\overline{\nabla \cdot \left[\alpha\overrightarrow{q_g'}\right]} \Rightarrow q_{ig} + q_{wg} \tag{8}$$

The momentum equation is transformed to the following under the third approximation:

$$\frac{\partial\left[(1-\alpha)\rho_l\overrightarrow{V_l}\right]}{\partial t} + \nabla \cdot (1-\alpha)\rho_l\overrightarrow{V_l}\overrightarrow{V_l} + (1-\alpha)\nabla P = \overrightarrow{f_i} + \overrightarrow{f_{wl}} + (1-\alpha)\rho_l\vec{g} - \Gamma\overrightarrow{V_i} \tag{9}$$

$$\frac{\partial\left[\alpha\rho_g\overrightarrow{V_g}\right]}{\partial t} + \nabla \cdot \alpha\rho_g\overrightarrow{V_g}\overrightarrow{V_g} + \alpha\nabla P = \overrightarrow{-f_i} + \overrightarrow{f_{wg}} + \alpha\rho_g\vec{g} + \Gamma\overrightarrow{V_i} \tag{10}$$

where force terms f_i, f_{wl}, f_{wg} represent shear force at the phase interface, the wall shear force acting on the liquid, and the shear force acting on the gas, per unit volume respectively. The term V_i responsible for the flow velocity at the phase interface (U. S. NRC 2007).

The final energy equation form under the forth approximation and the defining of the force terms is provided below:

$$\frac{\partial\left[(1-\alpha)\rho_l\left(e_l+\frac{V_l^2}{2}\right)\right]}{\partial t}+\nabla\cdot\left[(1-\alpha)\rho_l\left(e_l+\frac{P}{\rho_l}+\frac{V_l^2}{2}\right)\overrightarrow{V_l}\right]= \\ =q_{il}+q_{wl}+q_{dl}+(1-\alpha)\rho_l\vec{g}\cdot\overrightarrow{V_l}-\Gamma h_l'+\left(\overrightarrow{f_i}+\overrightarrow{f_{wl}}\right)\cdot\overrightarrow{V_l} \tag{11}$$

$$\frac{\partial\left[\alpha\rho_g\left(e_g+\frac{V_g^2}{2}\right)\right]}{\partial t}+\nabla\cdot\left[\alpha\rho_g\left(e_g+\frac{P}{\rho_g}+\frac{V_g^2}{2}\right)\overrightarrow{V_g}\right]= \\ =q_{ig}+q_{wg}+q_{dg}+\alpha\rho_g\vec{g}\cdot\overrightarrow{V_g}-\Gamma h_v'+\left(\overrightarrow{-f_i}+\overrightarrow{f_{wg}}\right)\cdot\overrightarrow{V_g} \tag{12}$$

The mass equation for the two-fluid model modifies to:

$$\frac{\partial[(1-\alpha)\rho_l]}{\partial t}+\nabla\cdot\left[(1-\alpha)\rho_l\overrightarrow{V_l}\right]=-\Gamma \tag{13}$$

$$\frac{\partial(\alpha\rho_g)}{\partial t}+\nabla\cdot\left[\alpha\rho_g\overrightarrow{V_g}\right]=\Gamma \tag{14}$$

The closure of the above mentioned equations is required. It is possible to achieve by using thermodynamic relations together with phase change and heat source correlations. A heat conduction limited model can be used in order to express the phase-change rate.

$$\Gamma=\frac{-(q_{ig}+q_{il})}{(h_v'-h_l')} \tag{15}$$

where q_{ig} and q_{il} terms are the interfacial heat transfer per unit volume on the gas and liquid respectively.

$$q_{ig}=\frac{P_v}{P}h_{ig}a_i(T_{sv}-T_v) \tag{16}$$

$$q_{il}=h_{il}a_i(T_{sv}-T_l) \tag{17}$$

Heat fluxes closure is accomplished by assumption of the form for the wall heat-transfer terms in following manner:

$$q_{wg} = h_{wg} a_w \left(T_w - T_g\right) = q'_{wg} a_w \tag{18}$$

$$q_{wl} = h_{wl} a_w (T_w - T_l) = q'_{wl} a_w \tag{19}$$

Force terms f_i, f_{wl}, f_{wg} expressed in the following way with relation to friction coefficients C_i, C_{wl}, C_{wg}.

$$f_i = C_i \left(\overrightarrow{V_g} - \overrightarrow{V_l}\right) \left|\overrightarrow{V_g} - \overrightarrow{V_l}\right| \tag{20}$$

$$f_{wg} = -C_{wg} \overrightarrow{V_g} \left|\overrightarrow{V_g}\right| \tag{21}$$

$$f_l = -C_{wl} \overrightarrow{V_l} \left|\overrightarrow{V_l}\right| \tag{22}$$

In the absence of practicability, the virtual mass terms were neglected. However, the further development of the TRACE code may require in future reconsideration regarding to virtual mass terms. Currently, sub-channel analysis of a reactor core is not available because of a simplification related to lift forces perpendicular to the flow, which were ignored. Representation of such terms can be vitally important for specific tasks.

In summary of the TRACE code overview, in the chapter were elucidated very basic foundations by which the code is working. As every computational tool, TRACE has its own limitations on applicability. Basically, the code is valid for LWR facilities investigations during accidental occurrences with some exceptions in reference to the current level of development of the program and peculiar reactor constructions. The code belongs to the type of codes using six equations approach with one dimensional modelling manner, including the opportunity of the three dimensional modelling for some components. Two-fluid modelling approach makes the code capable of treating the mechanical and thermal nonequilibrium at the same time. The discretization concept based on splitting components of a system on a number of control volumes, where the core of every control volume is intended for scalars, whereas edges of the control volume are destined for vectors. More comprehensive knowledge of TRACE fundamentals is available in TRACE theory manual.

4 TRACE MODEL OF PWR PACTEL FACILITY

The computational model of PWR PACTEL facility is represented as an aggregate of TRACE code elements conceptually repeating the construction of real facility. The model contains such major elements of the primary side as reactor core, upper plenum, pressurizer, hot legs, heat exchange tubes, cold legs, downcomer, lower plenum, and elements of the secondary side: feed water input, secondary side downcomer, risers, steam dome of the steam generators. The assembled representation of the computational model is shown in Figure 10.

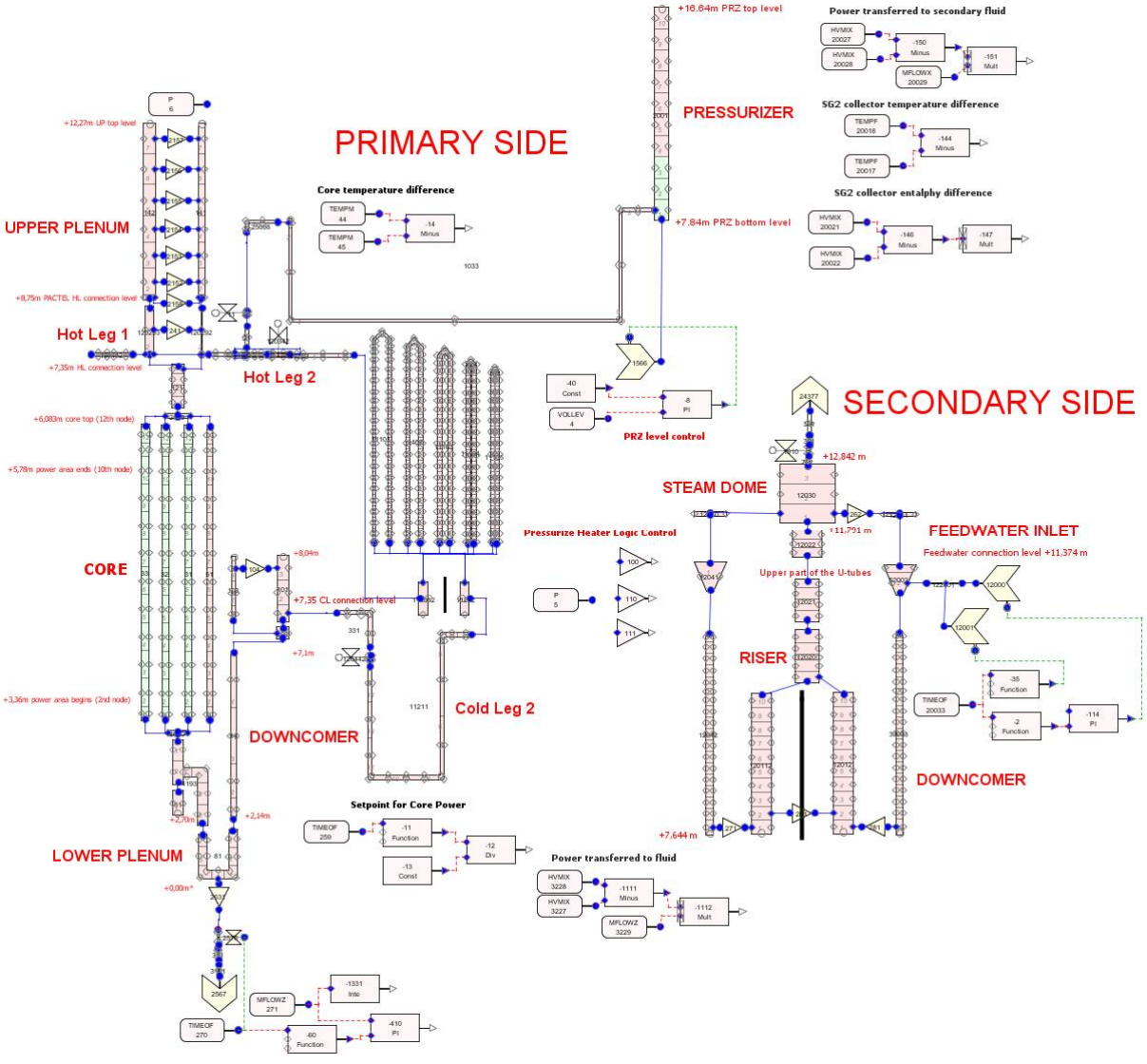

Figure 10: The assembled representation of the computational model of the PWR PACTEL facility (Loop 2)

On the Figure 10 the only Loop 2 is represented. The Loop 1 is built by the same principle apart of the presence of the pressurizer connection in this loop. The computational model has number of simplifications in reference to experimental facility. For instance, all the elements of the system are represented as pipes elements. Thus, the water channel in between core heat elements sections is a pipe element of the program. Concerning to the heat exchange U-shape tubes, in the facility there are 52 tubes divided in 5 groups by difference in length among those tubes. However, the computational model has only 5 heat exchange tubes where each tube represents the whole group of tubes with the same size, in every loop. Nevertheless, such principle points of the constructions as the shape of the cold leg are respected. The bottom elevation in the model is considered to be from the bottom of the pipe 81, U-shape pipe of the lower plenum in Figure 10. The pipe diameter is 0.14 m and thus, 0.07 m is added in above elevation values.

4.1. Primary side

In the designed TRACE model of the PWR PACTEL facility all of the elevation points of different parts coincide with those of experimental construction. The highest elevation point of the facility is considered to be at 16.64 m, which is the top point of the pressurizer as in the facility, thus in the computational model. As it was mentioned before, there are some simplifications had to be made, in order to streamline computing. Thus, in the primary side, the most perceptible simplifications refer to the core and heat exchange U-tubes.

Regarding to the core of the TRACE model, it is represented as the four pipe assembly. Three of those pipe elements represent core heat section each. They are marked with green color filling, as it shown on the Figure 10. The same heat element structure belongs to the pressurizer. In such a manner, the first three nodes of the pressurizer pipe component are filled with green color, which means that they are heat elements. Each node is responsible for one out of three groups of the pressurizer's heating elements.

Because of the triangular pitch in heat exchange tubes, there is the length difference between different tubes. Formally, to be accurate, the tubes need to be divided in ten groups, because of their length. Though in computational model there are only five groups. As long as TRACE

code does not allow round shapes, there are compromises were found. Thus, U-shape bends in each tube is made by turning nodes on 45 degrees angle. This modelling step is made by founding compromises between such three points as total length, length of U-shape bend and tube ceiling dimensioning.

The upper plenum part was significantly revised from the previous versions of it. In the current version of the upper plenum part there is a “pseudo-annular” channel was created between hot leg connection and upper plenum with pipe components. Upper plenum consist of two parallel flow channels, which connected to each other as it is shown in Figure 11.

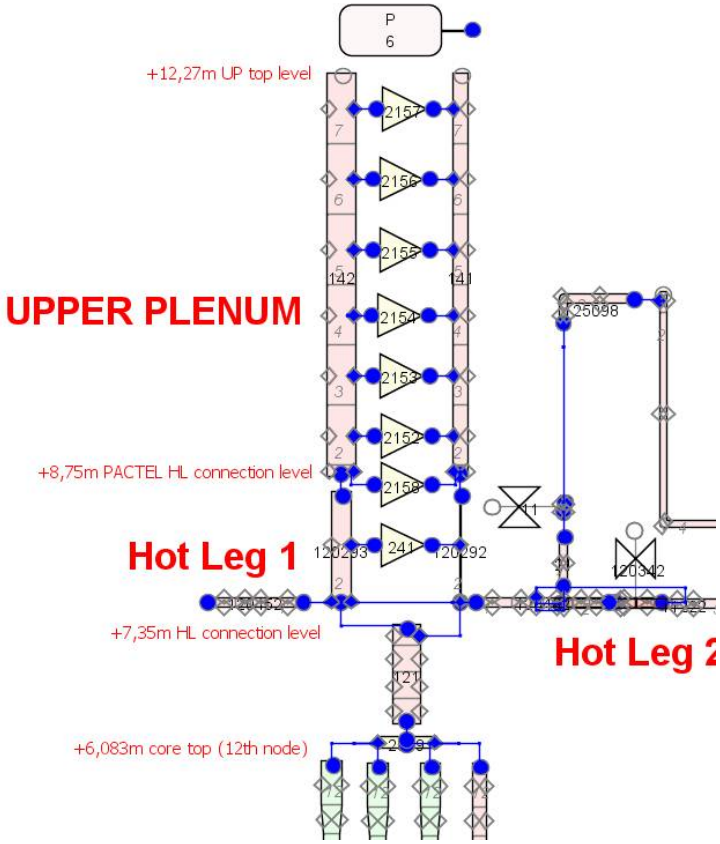

Figure 11: Configuration of the upper plenum model

4.2. Secondary side

The secondary side contains such main parts as feedwater inlet, downcomer, riser, steam dome and steam outlet. The modelling of the feed water inlet system is made by using a fill component. The fill component allows adjusting only a velocity inlet, and therefore mass flow is

handled by level controller element. The connection between the fill component and downcomer is arranged by a pipe component. The downcomer is divided into hot and cold sections, and the connection of the feedwater pipe is implemented to the cold side. Cold side of the downcomer is contemplated for feedwater downwards flow. In its turn the hot downcomer is envisaged for the steam dome condensation water brings down through holes. The hot downcomer is connected from the top to the steam dome and from the bottom to the hot riser. Accordingly the cold downcomer is joined to the feedwater inlet system on the top and to the cold riser at the bottom. Riser parts are also implemented as pipe components. There are five riser parts: hot and cold risers, one common element with heat exchange tubes, one riser element with the top points of U-shape bands of tubes and on riser element without tubes.

5 EXPERIMENTS DESCRIPTION

5.1. Natural circulation

Natural circulation is considered as an imperative core cooling mechanism in NPP in cases of accidents or transients accompanied with loss of forced circulation. In the early stages of reactor startups as well as after shutdowns, the mechanism of natural circulation ensures cooling of the system. In cases of accidents on a NPP, natural circulation may be the only possible tool for decay heat removal. There are several possible ways of the cooling system recourse to natural circulation mode: a loss of off-site power, failure of a reactor coolant pump or a deliberate turni-off of forced cooling systems by an operator. In every case, the density difference between the medium leaving the heat source at one elevation and the low-temperature receiver at higher elevation will create a currant of that medium, which will provide a passive core cooling effect. The overall behaviour along with cooling efficiency by natural circulation are directly related to flow regime of the primary circuit, which, in its turn, depends on core power and coolant inventory. For a SBLOCA scenario, the dependence between general behaviour of natural circulation mechanism and coolant inventory is one of the most important characteristics, because in such type of accidents the core cooling is required at significantly reduced inventory.

The mass flow rate that takes place during natural circulation is a function of the balance between the buoyancy forces and the frictional forces. The buoyancy forces drive the flow and vary with such factors as the fluid density difference between hot and cold leg sides and the elevation difference of the heat source and the low-temperature receiver. In cases of unchangeable elevation points of the heat and sink sources there will not be influence on the value of buoyancy forces and the only density difference will determine a degree of those forces. Therefore, there is the directly-proportional dependence between fluid density difference and buoyancy forces. By the same token, the frictional forces differ according to the loop geometry and the nature of the liquid. As long as the loop geometry is fixed, thus the frictional forces very with only the nature of the liquid. Frictional forces are higher for two phase mixture flow rather than for subcooled or saturated single phase liquid flow. Likewise, the flow pattern along with void fraction at a large extent determine rate of the frictional forces.

The actuating medium flow rates during natural circulation mode notably lower than those during normal reactor operation. During emergency conditions for PWR's, a distinction is made between modes of natural circulation on three types. In such a manner, each mode depends on the primary coolant quality, which depends on the coolant inventory of the loop.

While the primary coolant inventory is contained in full scale, it represents the first mode of natural circulation of saturated single phase actuating medium. With the appearance of a leakage in the primary circuit the transition from the single phase liquid flow to the two phase mixture flow is taking place, which by convention means the presence of the second mode of natural circulation. In the core area vapor phase originates and in the steam generators the condensation occurs. The exact moment of the transition from single phase flow to the two phase flow happens after decreasing of the water level in the upper plenum lower the elevation of hot leg connection, which makes it possible for vapor phase to permeate to the primary circuit flow. Inasmuch as the permeant steam is increasing the density difference of the flow between the core and the steam generator, therefore mass flow rate rises. With the reduction of the medium inventory of the primary side, void fraction increases and steam bubbles now reach downstream area of U-shape heat exchange tubes. The apex of maximum possible flow rate values is reached when boundary of the single and two phase flow is located at the top point of U bend of heat exchange tubes.

The third natural circulation mode one may associate with conditions of the system when primary coolant inventory is significantly reduced. Under such conditions, the flow of the actuating medium can be categorized as boiler condenser or reflux condensation flow. That occurs when liquid no longer possible to overcome the U-bend of heat exchange tubes. In such case, the primary coolant is circulating primarily in the form of the steam flow from the core to the steam generator. Fraction of the steam currant condenses in the steam generator whereupon the condensate flows back to the core through the hot leg as counter current flow and the rest returns to the core through the cold leg. Nevertheless, if the velocity of the steam current is high enough, then liquid may stay in the up flow side of the steam generator heat exchange tubes. Liquid level increases in both sides of the tube, as the steam plug becomes smaller resulting from condensation. Instantly after liquid in upstream side reaches the top of the U-

bend, there is a quick drop of mixture into downstream side occurs. Such mode is called fill and dump mode.

In the first two natural circulation modes the heat removed from the core differs according to the core power rate and the mass flow rate within the loop. In fill and dump mode the heat removal efficiency strongly depends on the capacity of the steam generators to condensate the steam in primary circuit. Which natural circulation mode will take place during accidents related to loss of coolant mainly depends on primary coolant inventory. However, not least important is values of primary and secondary pressures as well as their difference. In connection with this, a variety of experiments dedicated to research of natural circulation under conditions of inventory reduction were implemented. Such experiments offer opportunities to estimate system cooling capabilities over a wide range of conditions. Thus, in the current work there are two types of experiments examined: Stepwise Inventory Reduction (SIR) and a Small Break LOCA (SBL) experiments.

5.2. Stepwise Inventory Reduction experiments

Stepwise inventory reduction experiments were executed in order to observe the natural circulation flow behavior over quasi steady state conditions upon a variety of primary side inventory levels. Throughout the performed experiments the classification may be made on conditionally high pressure (SIR-31), medium pressure (SIR-32), and low pressure (SIR-33) experiments. All three experiments have principal similarities of the procedure apart of some details. Hence, for all SIR experiments the core power were established on the level of 115 kW approximately. Such heating power is equal to 1.1% scaled nominal power in the reference reactor. In each experiment the steady state of 1000 seconds was sustained. The experiments were run by utilizing only one loop of the facility (loop II), while the loop I was isolated from the system. The initial conditions of the experiments provided below in corresponding tables. After the steady state, the heaters of the pressurizer were turned off as well as the pressurizer was isolated from the primary circuit by using the isolation valve, which is installed in the pressurizer surge line. This was done in order to avoid changings of the inventory because of possible fluid flow in and out of the pressurizer.

5.2.1. SIR-31

Table 5: Initial conditions in SIR-31 experiment

PARAMETER	***VALUE***
Primary side pressure	75 bar ± 1 bar
Secondary side pressure	42 bar ± 0.6 bar
Core power	115 kW ± 6 kW
Steam generator collapsed level	3.9 m ± 0.12 m
Loop mass flow rate	0.75 kg/s ± 0.14 kg/s

After the isolation of the pressurizer, the primary coolant was blown down in several steps through a sharp-edged orifice with 3.5 mm in diameter located in the lowest elevation point of the lower plenum. The technical performance of the break is shown in the Figure 12.

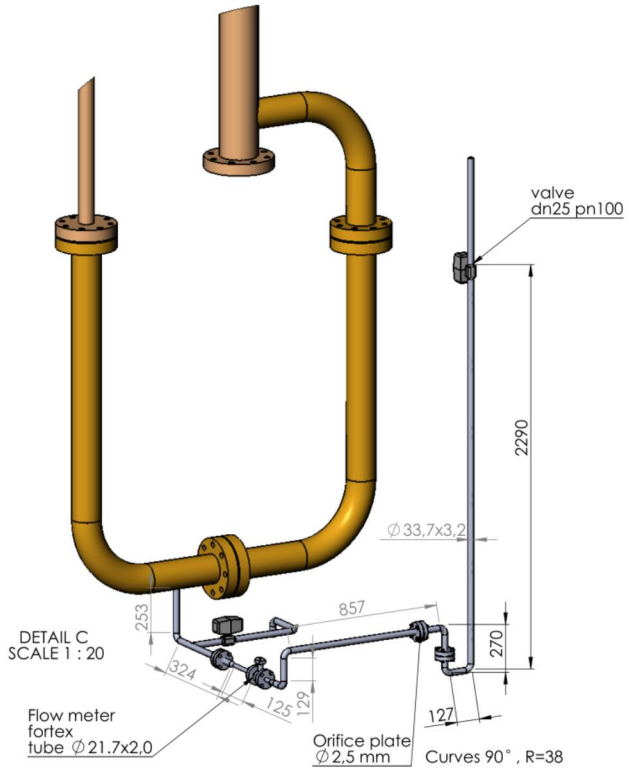

Figure 12: Location and technical performance of the break

Each next step of draining the primary coolant occurs with 1000 seconds period in between. In the first blow down step approximately 45 kg of working medium were extracted out of the system. In the second draining step it took 40 kg. Including the third draining step, in each

next step, the amount of retrieved coolant was 30 kg. Throughout the duration of the experiment the secondary side parameters were maintained unchangeable. The experiment was finished at the point when the primary coolant inventory was depleted insomuch that the core temperature exceeded 350 ℃.

5.2.2. SIR-32

Table 6: Initial conditions in SIR-32 experiment

PARAMETER	***VALUE***
Primary side pressure	40 bar ± 1 bar
Secondary side pressure	20 bar ± 0.6 bar
Core power	115 kW ± 6 kW
Steam generator collapsed level	3.9 m ± 0.12 m
Loop mass flow rate	0.73 kg/s ± 0.14 kg/s

The procedure of the SIR-32 experiment is the same as it was described above. However, it has some quantitative differences. Thus, the orifice diameter is 2.5 mm. The amount of drained out working medium in the first step is 50 kg, in the second step it is 45 kg and in each next step it is about 40 kg. Each step occurs in 1000 seconds after the beginning of the previous step. Apart from these differences in the numerical values, the procedure of the experiment is the same as in SIR-31.

5.2.3. SIR-33

Table 7: Initial conditions in SIR-33 experiment

PARAMETER	***VALUE***
Primary side pressure	20 bar ± 1 bar
Secondary side pressure	10 bar ± 0.6 bar
Core power	115 kW ± 6 kW
Steam generator collapsed level	3.9 m ± 0.12 m
Loop mass flow rate	0.73 kg/s ± 0.14 kg/s

The only difference in the procedure of the SIR-33 experiment compare to the SIR-32 experiment is the amount of drained primary coolant in each step. Thus, in the first step only 45 kg of medium were drained and in each next step it was approximately 40 kg per each 1000 second step.

5.3.Small Break LOCA experiment

The small break LOCA experiment (SBL-50) was performed in order to observe the natural circulation behavior through a continuous range of primary side coolant inventories. The initial conditions of the experiment and its procedure are provided below.

5.3.1. SBL-50

Table 8: Initial conditions in SBL-50 experiment

PARAMETER	***VALUE***
Primary side pressure	75 bar ± 1 bar
Secondary side pressure	42 bar ± 0.6 bar
Core power	155 kW ± 6 kW
Steam generator collapsed level	3.9 m ± 0.12 m
Loop mass flow rate	0.6 kg/s ± 0.14 kg/s

The experiment starts by 1000 second steady state with full amount of the primary coolant inventory. After that a small break, installed in the cold leg of loop II is opening and by that initiate a slow inventory reduction. There are two loops of the facility in use for the experiment. The orifice diameter, through which leakage occurs, is 1 mm. The break is installed in between the loop seal of the cold let and the downcomer on the top side of the pipe. As in the stepwise inventory reduction experiments, upon reaching the end of the steady state, the pressurizer was isolated from the primary side by the isolating valve, its heaters were switched off, following which the opening of the orifice occurred. By the end of the experiment nothing else was undertaken. The experiment was considered finished after the exceeding of the core temperature in 350 ℃.

During the experiment an unintentional closing of the break took place, because of the valve malfunctioning. It was fixed within roughly 20 minutes.

6 CALCULATION RESULTS

In the current chapter, results of the experiments compare to computational simulation results. Among parameters in question there are drained mass from the primary side, collapsed water level in the primary side, mass flow in loops, pressures in the primary and secondary side, temperature in core inlet and outlet, temperature in upper plenum top and bottom sides.

6.1. Stepwise Inventory Reduction experiments

Throughout all three SIR experiments, primary circuit pressure significantly falls down after the first act of primary coolant extraction (Figure 16, 23 and 30), which causes boiling in the core (Figure 17, 19; 24, 26; 31, 33). The water in the top of the upper plenum instantaneously evaporates. The primary circuit pressure rises because of the generated steam in the core. The second extraction of working medium leads to drop of the collapsed liquid level in the upper plenum close to the hot leg connection elevation (Figure 14, 21 and 28). In 1000 seconds after that, the third step occurs, where for all three experiments, an inherent primary pressure drop taking place. By that moment, the overall amount of drained coolant is large enough for the collapsed liquid level falls down below the hot leg connection elevation, which allows the steam formed in the core to flow into the hot leg.

Considering that now newly generated steam has option to leave reactor through hot leg, the core outlet temperature critically goes down. It can be observed from graphs (Figure 19, 26, 33), that since the first draining step to the third step, the steam in the top part of the upper plenum is superheated. That happens by reason of presence of metal-intensive flanges on the upper plenum top part. Cooling rate of them is lower than the rest of other parts of the facility. Thus, the temperature of the upper plenum is higher than other temperatures in the facility.

In conjunction with mass flow dynamic within the hot leg, at the start of a SIR experiment (Figure 15, 22, 29), the working medium has the phase state of subcooled single phase water. After each draining step until the third blow down there are specific jumps of mass flow rate in the hot leg. It can be explained by reaching the steam bubbles having occurred into the coolant flow, which appeared in consequence of water to steam flash in the upper plenum and

dragged down to the stream with steam bubbles from boiling in the core. Because of that reason, the density of the upstream side of the natural circulation loop decreases, which in its turn leads to mass flow rate jumps. Until the third drain step, drawn into the flow steam bubbles condense in the hot leg. Apart from the jumps in mass flow rate function, before 3000 seconds the tendency in overall level of the mass flow rate stays without changes. However, since the collapsed fluid level drops lower the hot leg elevation, the generated steam has no restrictions to flow freely into hot leg. That is why after the third draining step, mass flow rate does not stabilize on the same level as it was in the previous times. After the fourth extraction of the working medium the results differs from experiment to experiment. In SIR-31 and SIR-32 experiments after 4000 seconds, the dramatic drop of the mass flow rate follows. On the other hand, in SIR-33, it happens 1000 seconds later. Such tremendous drop ushers in the transition to the boiler condenser or reflux condensation mode. By that moment, not even collapsed liquid level is lower of the hot leg elevation, but also the swell level now is well below this point. It means that now, inside the hot leg enters only the steam, which condenses in the steam generator area of heat exchange tubes. Depending on the steam velocity value, the condensate in upstream side either goes back by countercurrent flow with low steam velocities or pushes to the downstream side of the loop.

6.1.1. SIR-31

In order to achieve objective simulation results, besides initial conditions such as primary and secondary pressures, working mediums temperatures, there are procedural conditions had to be kept. Thus, the drained from primary side mass was one of the parameters causing the most interest. From the Figure 13 it can be observed that on each step of primary coolant extraction precisely the same amount of working medium was reached. Nevertheless, after the fourth draining step there is a difference in the draining time. According to experimental results, the medium was supposed to drain out of the system slightly faster in computational model. However, the results are promising.

From the mass flow rate function (Figure 15) in can be concluded that natural circulation was established in the loop. It is worth to mention that simulation results match very well until the fourth draining step, after which according to the experiment there was meant to be a transi-

tion to boiler condense mode of natural circulation. Yet still, it happened only with fifth drain. Even though amount of extracted medium of both: experimental and simulated characteristic curves matches well enough throughout the whole experiment, it appeared that decisive role belongs to the pressure dependences (Figure 16). Thus, during the period from 3000 to 4000 seconds, the mass flow rate functions (Figure 15) coincide to each other, despite on large primary pressure difference (Figure 16). After 4000 seconds, experimental primary pressure (Figure 16) drops lower than 45 bar, which only causes more vigorous boiling and therefore transition to reflux condensation mode (Figure 15). On the other hand, the primary pressure in the simulation after 4000 seconds not even reaches the same level as it was in the experiment and stays a bit higher (Figure 16). Such pressure remains the density of the steam in simulation higher than the density of the steam during the experiment. Thus, the boiling processes during period from 4000 to 5000 seconds are less vigorous.

In addition, the delay in transition to reflux condensation mode between simulation and experiment can be explained from collapsed liquid level perspectives (Figure 14). Therefore, the same water level as in the experiment transition during 4000-5000 seconds Figure 14, was reached in the simulation only after fifth draining step (5000-6000 seconds Figure 14).

The first draining step drops the primary pressure significantly. In the simulation results, this drop happens to be slightly lower. As a result of boiling after the first drain, forming steam increases the primary pressure. In the simulation this growth of pressure goes faster than in the experiment and by the second step, the numerical value of the primary pressure in the simulation is bigger. The second drain does not affect the system that much as the first step and the difference of the pressure between the simulation and the experiment remains the same until the third step. After 3000 seconds, there is one more rapid decrease of pressure. It can be observed that this second significant drop happens always after the collapsed liquid level drops below the hot leg elevation connection point. This statement is fair not only within the SIR experiments, but also for the SBL experiment. It can be illustrated by analyzing coupled graphs of collapsed liquid level (Figure 14, 21, 28) and primary pressure functions (Figure 16, 23, 30). After the fourth draining step, inaccuracy primary pressure values between the simulation and the experiment reduces and stays the same until the end of the experiment. The most

probable explanation for the divergence in primary pressure values between the simulation and the experiment is that heat losses were not simulated precisely.

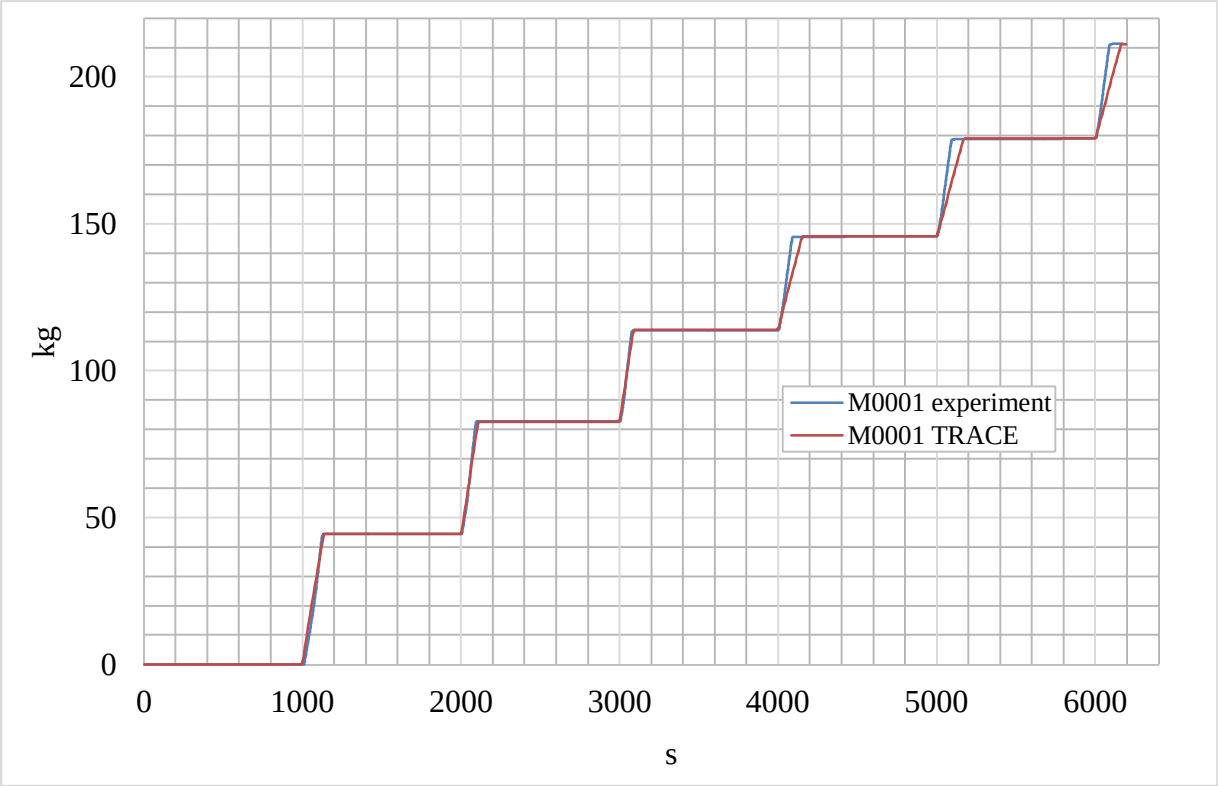

Figure 13: Simulation results versus experiment results, drained mass from the primary side, SIR-31 experiment

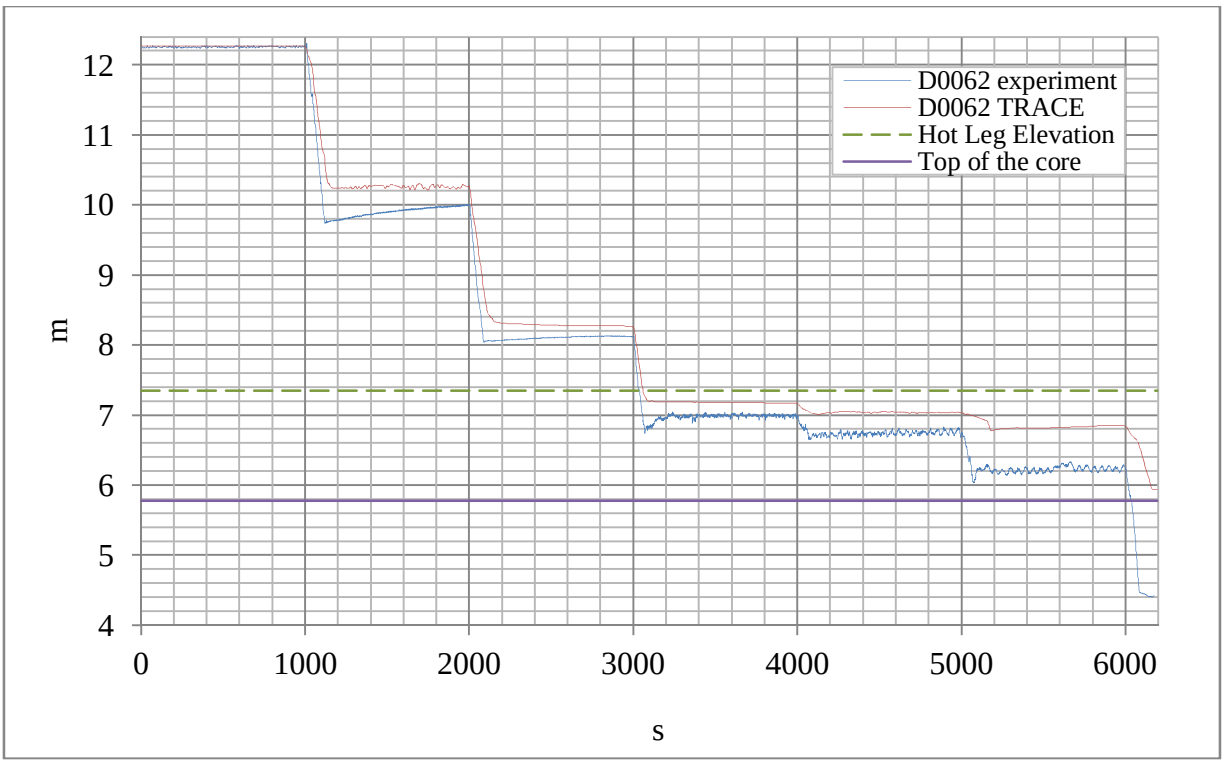

Figure 14: Simulation results versus experiment results, collapsed water level in the primary side, SIR-31 experiment

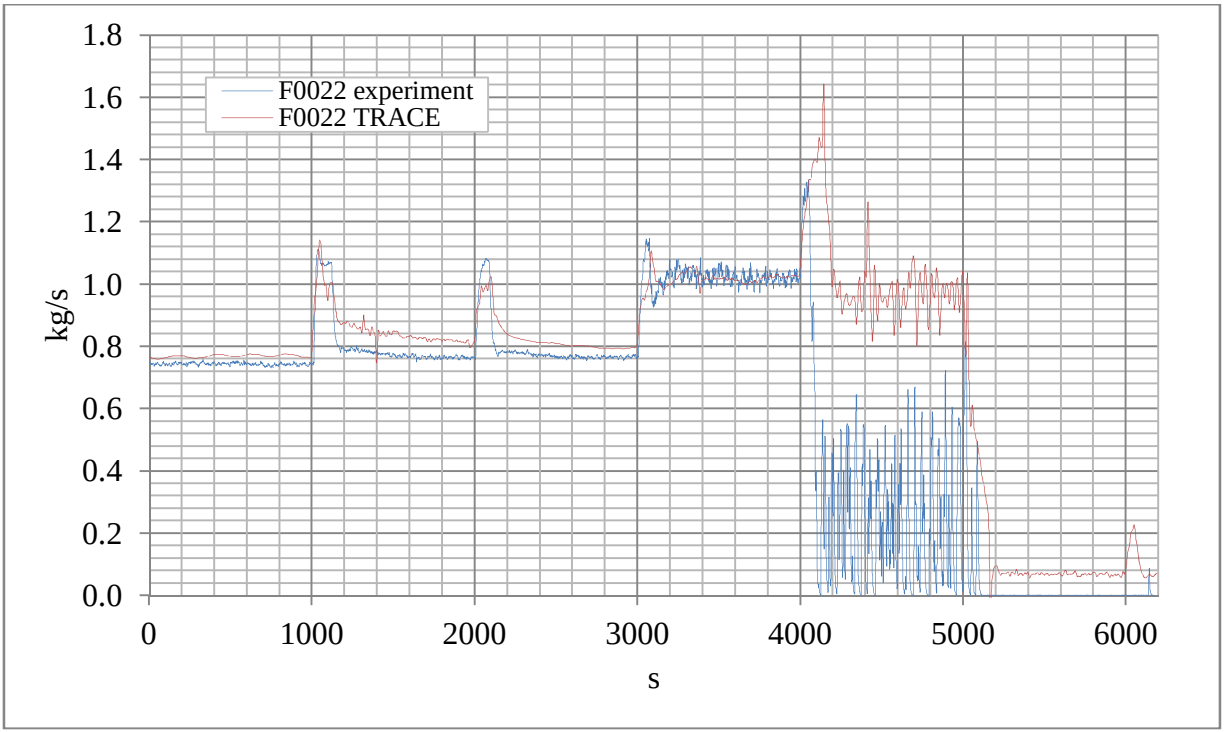

Figure 15: Simulation results versus experiments results, mass flow in loop II, SIR-31 experiment

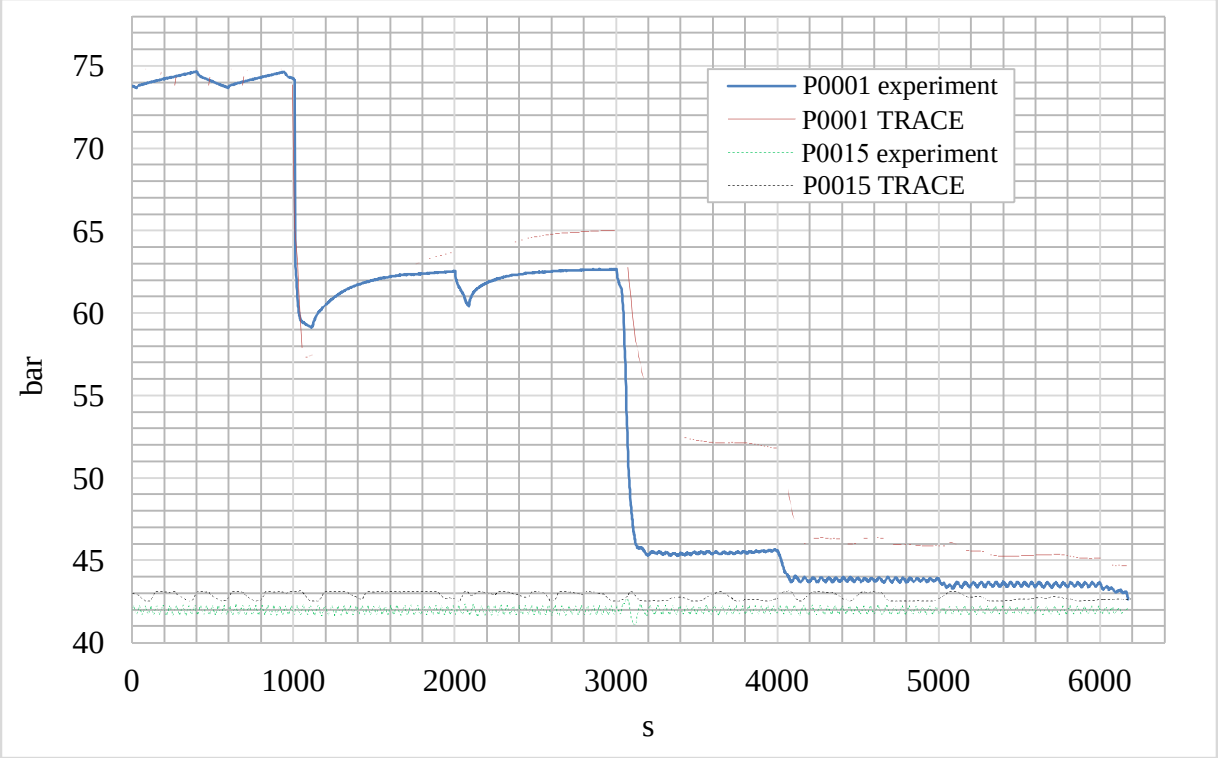

Figure 16: Simulation results versus experiment results, pressures in the primary and secondary side, SIR-31 experiment

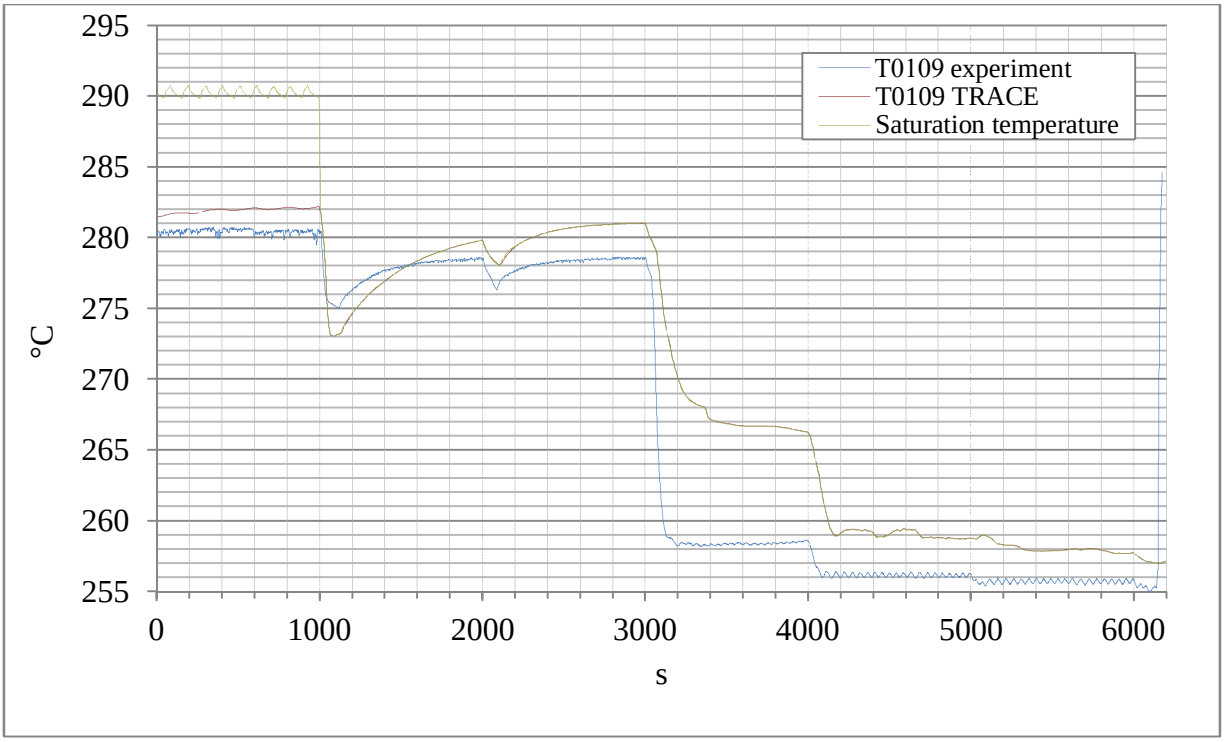

Figure 17: Simulation results versus experiment results, temperature in core outlet (channel A), SIR-31 experiment

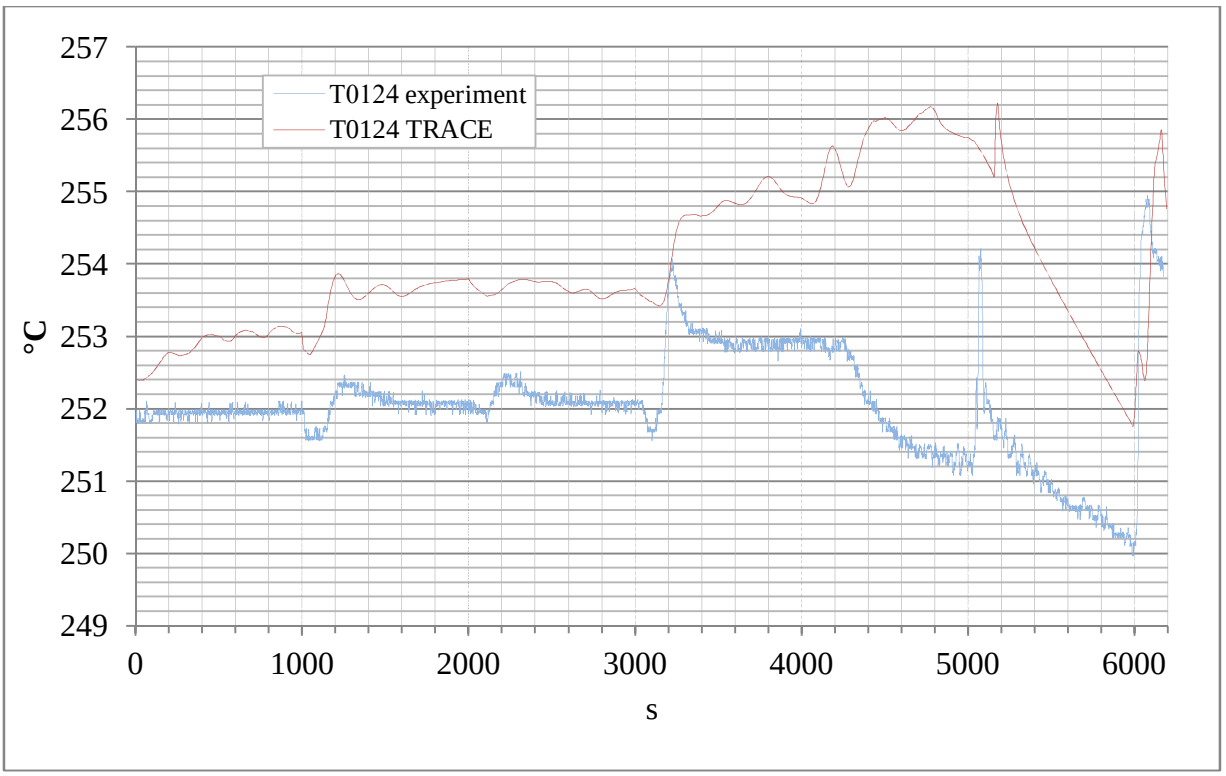

Figure 18: Simulation results versus experiment results, temperature in core inlet, SIR-31 experiment

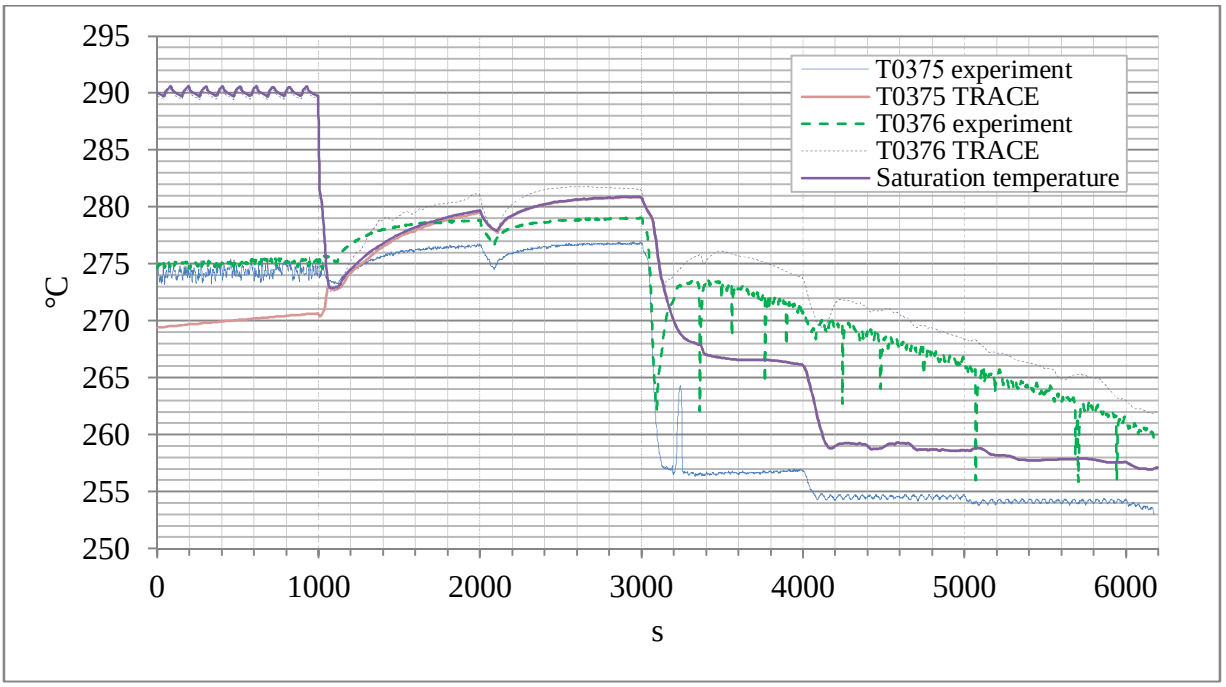

Figure 19: Simulation results versus experiment results, temperature in upper plenum (T0375 upper plenum bottom, T0376 upper plenum top), upper plenum top temperature is steam temperature, SIR-31 experiment

6.1.2. SIR-32

In reference to the SIR-32 experiment, it is worth to mention that the procedure was not followed through, as it was prerequisite. Figure 20 shows that the experiment starts much earlier and that steady state lasts not for 1000 seconds, but for 407 seconds. Along with this, the valve was not opened totally in the period from 407 to 1000 seconds. The prerequisite first step of primary coolant extraction occurs at 1000 seconds the valve opens totally. The same procedural inaccuracies are taking place in the period between the first and the second drains (Figure 20). It is also interesting to note that in each step in the simulation the primary coolant blows down noticeably slower. It can be related to friction properties of the break tuning. However, despite on mentioned above difficulties, on each step of the simulation roughly the same amount of drained out primary coolant was achieved.

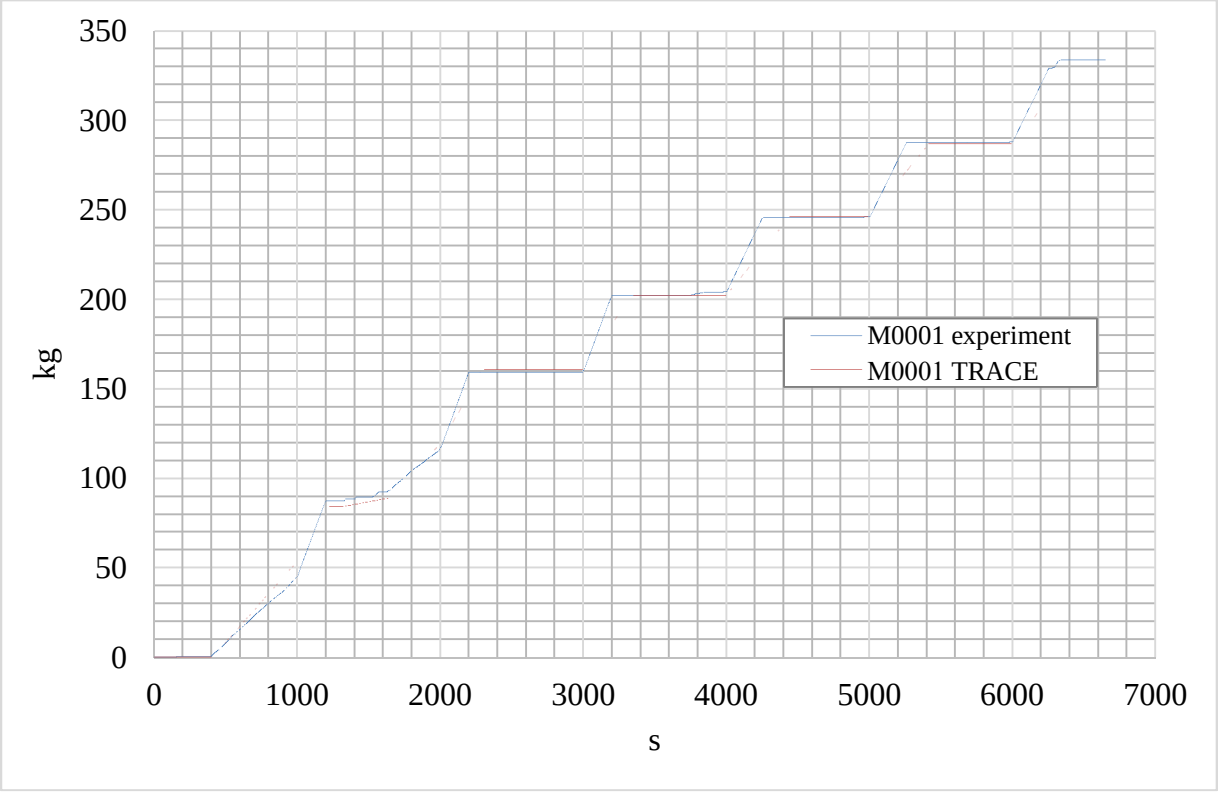

Figure 20: Simulation results versus experiment results, drained mass from the primary side, SIR-32 experiment

As it can be seen from the collapsed water level function (Figure 21), even though medium was started to drain out before the first official step, the level does not change as well as the primary pressure (Figure 26). By 1000 seconds, the amount of the extracted coolant was large enough to destabilize the system. However, it does not happened because of the connected to the primary circuit pressurizer, which by the procedure, isolates only after 1000 second steady state.

The collapsed water level simulation in 1000 to 3000 seconds period appeared not precise with the experimentally obtained results. Thus, after the first drain there is no steady water level as it was expected according to the experiment. In pursuance of the simulation results water level drops steadily throughout 1000 seconds after the first step and reaches the hot leg elevation connection point nearly. However, it stays higher that point, which keeps the primary pressure in the simulation roughly on the same level as in the previous one thousand period. Presumably, in order to achieve the elimination of such inaccuracy in the collapsed water simulation, one needs to reach better matching between the experiment and the simulation in the drained mass dependences. After the third drain, the collapsed water level in both: the experiment and the simulation drops below the hot leg elevation and the numerical values match relatively good.

In respect of mass flow in the second loop, it is worthwhile to say that all principal peculiarities of the flow within the simulation results appear at the same time as it is expected according to the experiment. Thus, until 3000 seconds, the simulation and the experiment results match relatively well. After the third drain, the increase of the mass flow rate happens, though numerical values are different for the simulation Figure 22. Such excess can be explained from the primary pressure changing perspective. In concordance with the Figure 23, during the third act of the primary coolant extraction, the primary pressure of the simulation drops from higher point of approximately 36 bar to the lower than in the experiment value. This difference in the pressure drop causes more vigorous boiling in the simulation and as a consequence dragging down to the stream of coolant more steam bubbles and therefore the increase in the mass flow rate larger than in the experiment.

Taken as a whole, it should be mentioned that for such parameters as the pressure and temperatures parameters of interest was achieved a good range of matching.

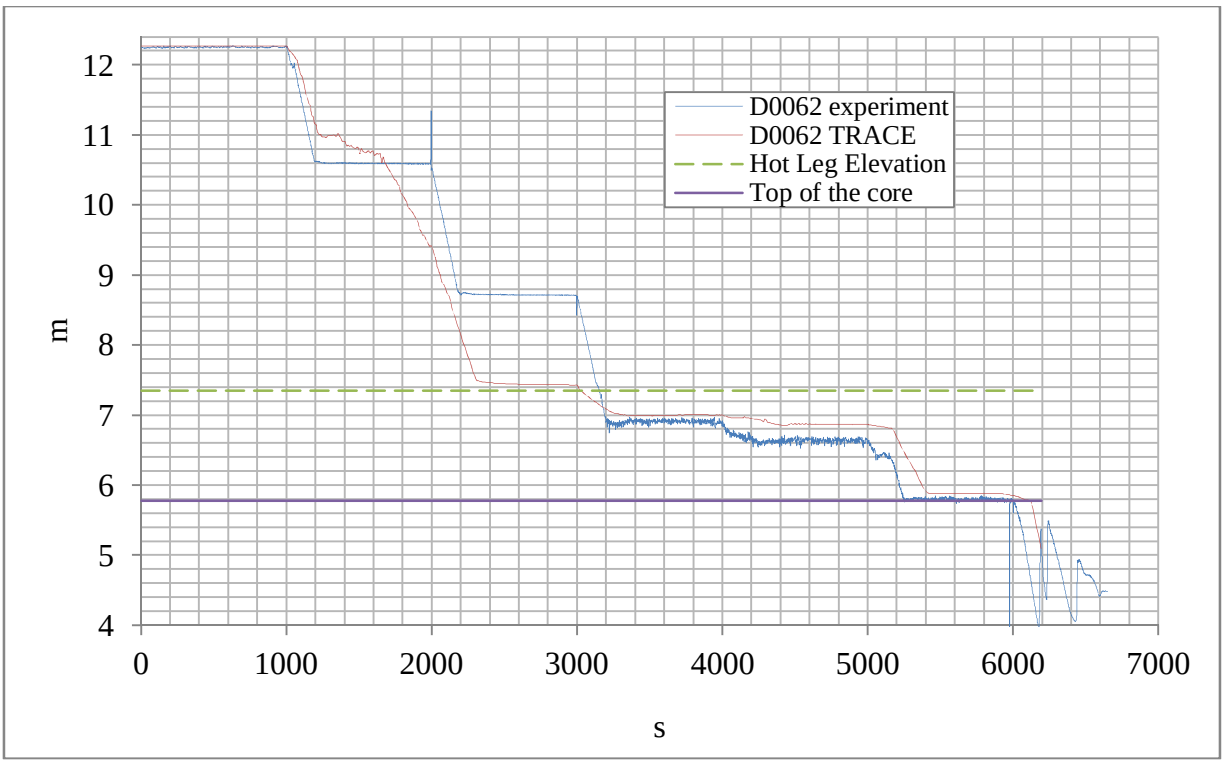

Figure 21: Simulation results versus experiment results, collapsed water level in the primary side, SIR-32 experiment

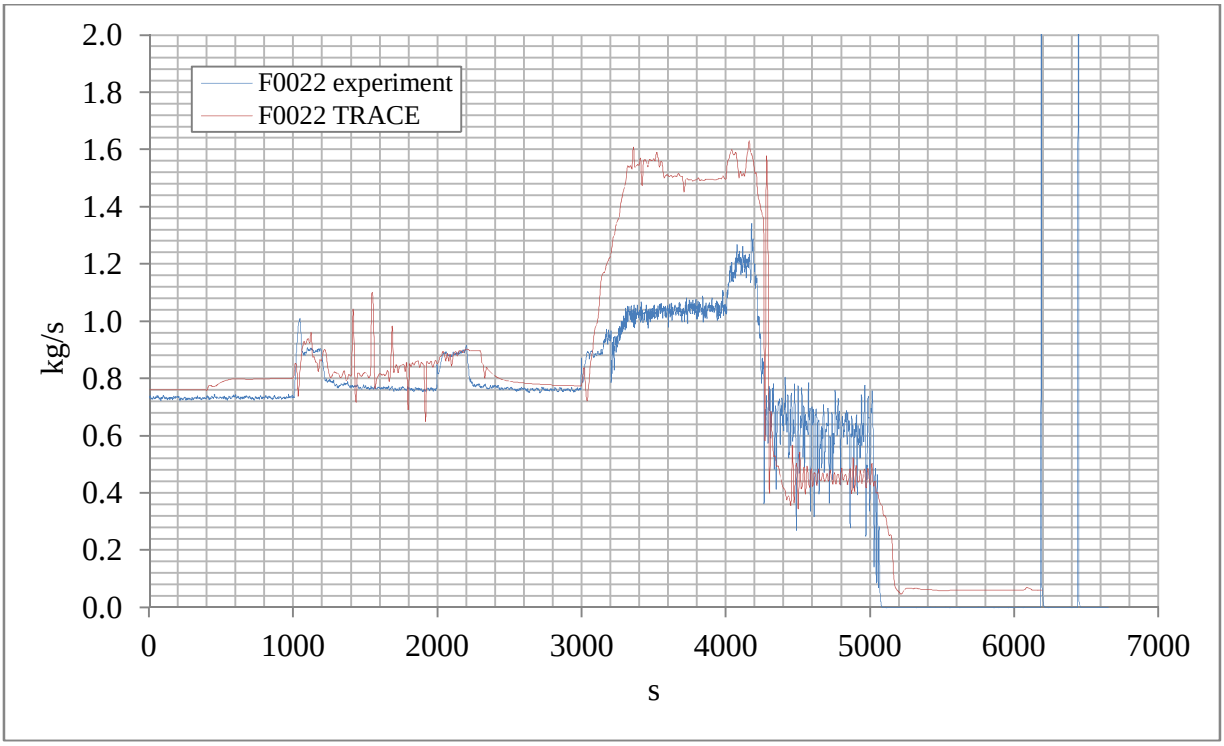

Figure 22: Simulation results versus experiments results, mass flow in loop II, SIR-32 experiment

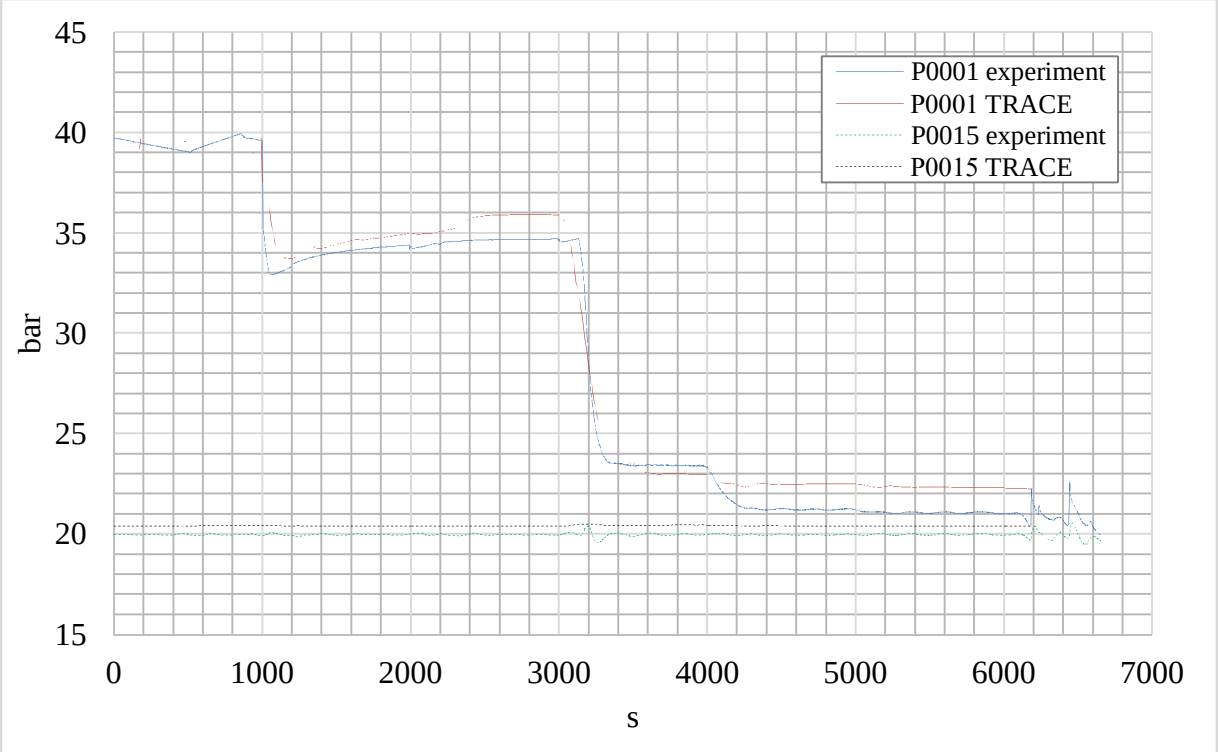

Figure 23: Simulation results versus experiment results, pressures in the primary and secondary side, SIR-32 experiment

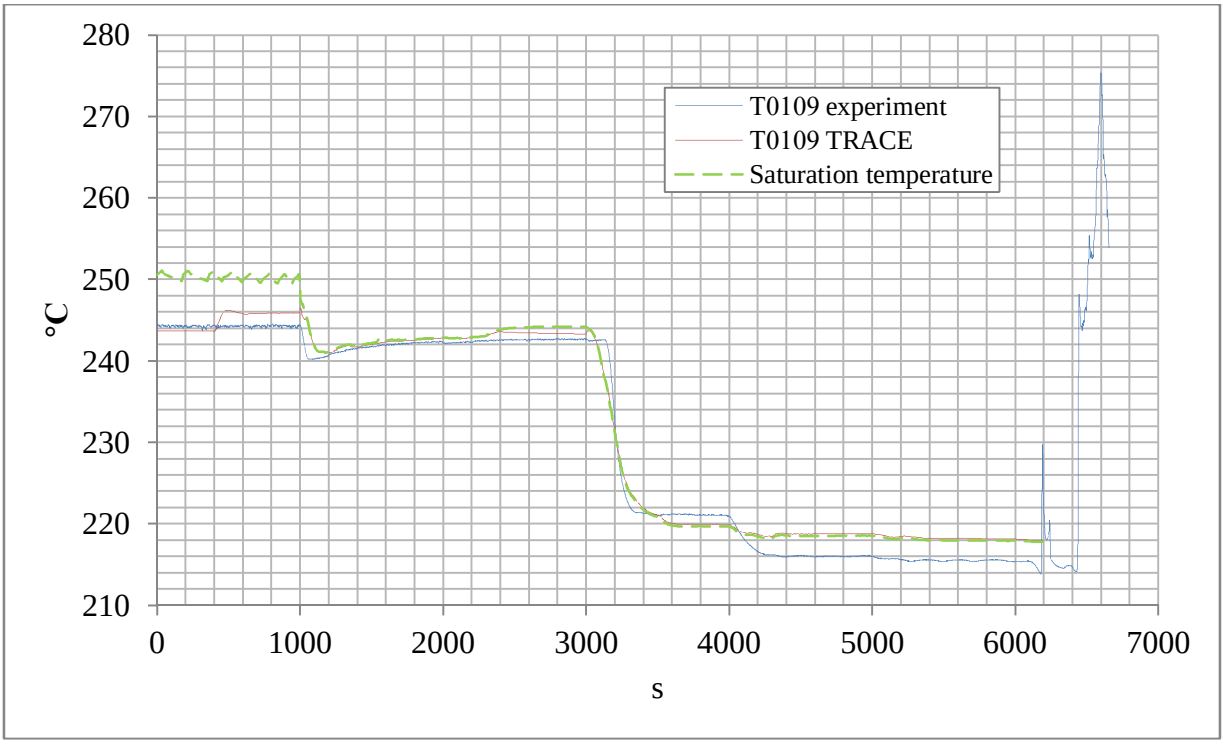

Figure 24: Simulation results versus experiment results, temperature in core outlet (channel A), SIR-32 experiment

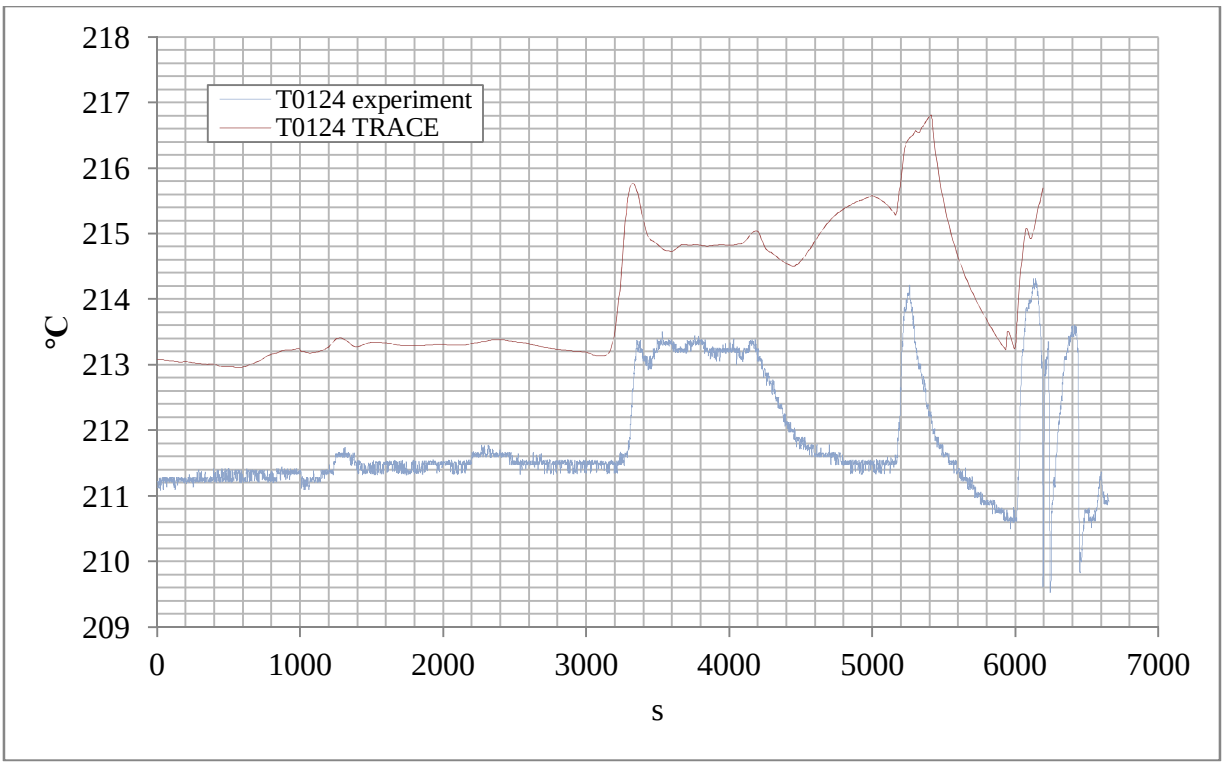

Figure 25: Simulation results versus experiment results, temperature in core inlet, SIR-32 experiment

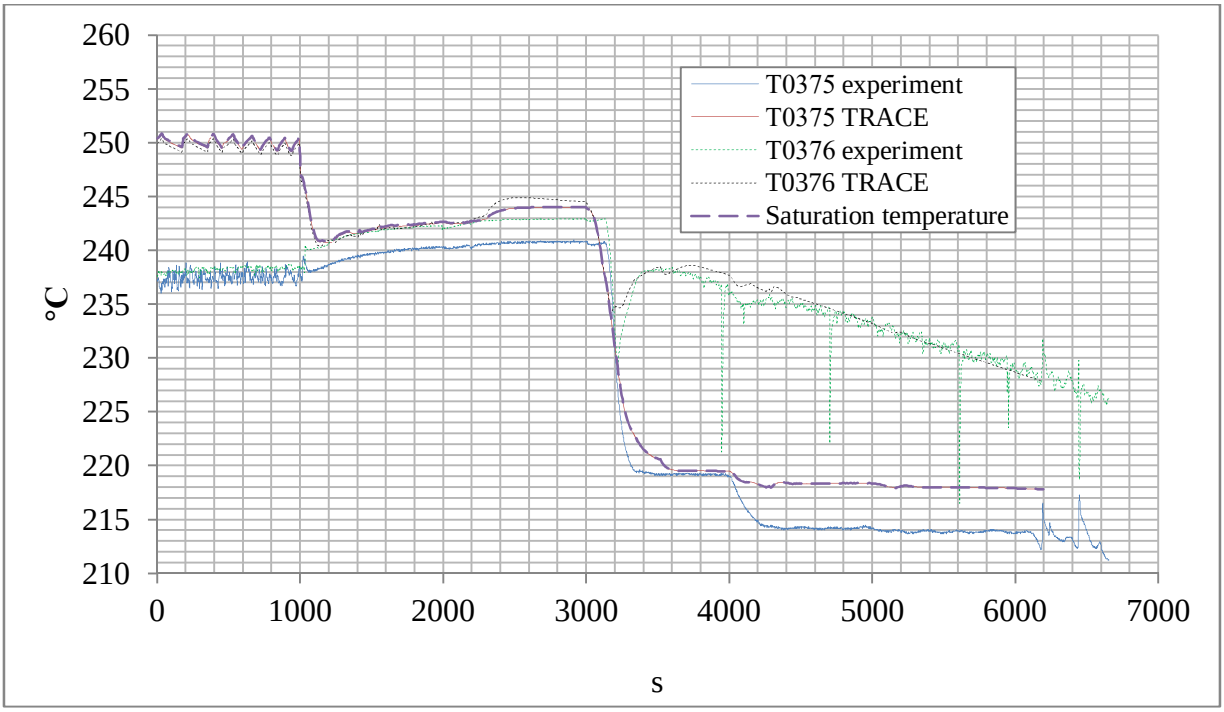

Figure 26: Simulation results versus experiment results, temperature in upper plenum (T0375 upper plenum bottom, T0376 upper plenum top), upper plenum top temperature is steam temperature, SIR-32 experiment

6.1.3. SIR-33

The SIR-33 experiment is, for the purposes of discussion, the experiment with low pressure. According to the results of the experiment, the average power of the core is 110 kW. During the simulation, it was revealed that under this condition along with the other initial conditions the computational model is not able to reach stable state. Such heat power of the core makes the system start to boil, before even the first draining. Thus, it was decided to find boundary core power condition when the computational model would behave adequately.

The calculations were made for six different values of core power. All of them are below 110 kW. For the power of 109 kW two different types of computing were made. The number 1000 next to 109 kW in the graph's legend means that for this very computing attempt the steady state period is equal to 1000 seconds. On the other hand, the number 2000 next to 109 kW sign means 2000 seconds period of the steady state.

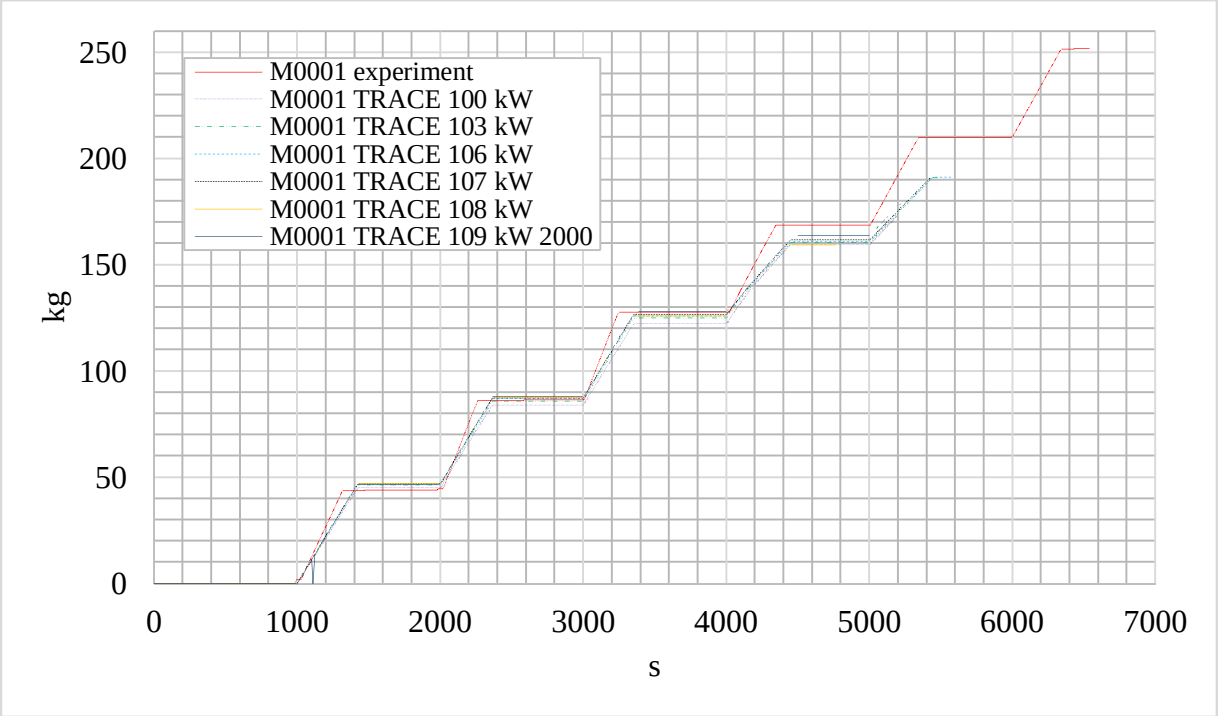

Figure 27: Simulation results versus experiment results, drained mass from the primary side, SIR-33 experiment

As it can be observed from the graphs in reference to the SIR-33 experiment, all principal phenomena are represented during the calculation. However, the numerical values between each attempt of the calculation vary. Thus, for the calculations where the power core equals to 108 and 109 kW the results are much less ideal.

According to the collapsed water level functions (Figure 28), it can be observed that «108 kW» and «109 kW 2000» calculations are unstable during the first 1000 seconds. The oscillations which are detected within this period have the tendency to increasing of the amplitudes. Thus, with long enough steady state period the system would not reach the steady state at all. One thousand seconds less steady state for 109 kW core power changes results radically. By doing that, one may conclude that those results for 109 kW 1000 matched rather well compared to the experimental results. However, this statement would be entirely faulty. Because as it was said before, for the experiment «109 kW 2000», during the steady state period of 2000 seconds system did not reach the steady conditions. Evidently, the time difference in steady state duration between experiment «109 kW 1000» and «109 kW 2000» makes a very big difference in the results. Therefore, one must to set the steady state period very carefully, especially in cases like this.

After analyzing obtained results, it can be said that the core power corresponding to 107 kW is the closest to the average original value in the experiment, when the computational model stable and behave according to the experimental results.

In conclusion, the simulation of the SIR-33 experiment was adjacent with some problems, which were overcome. However, there was a disability to simulate the exact same core power revealed. Thus, the core power according to the experimental data was 110 kW in average. Though, during the modelling it was possible to reach only 107 kW of the core power with remaining of all inherent experimental phenomena. In addition to that, in the period from 3000 to 4000 seconds, there is a noticeable inaccuracy in the primary pressure and temperatures between the simulation and the experiment. Apart from those imprecisions, the results can be considered satisfactory.

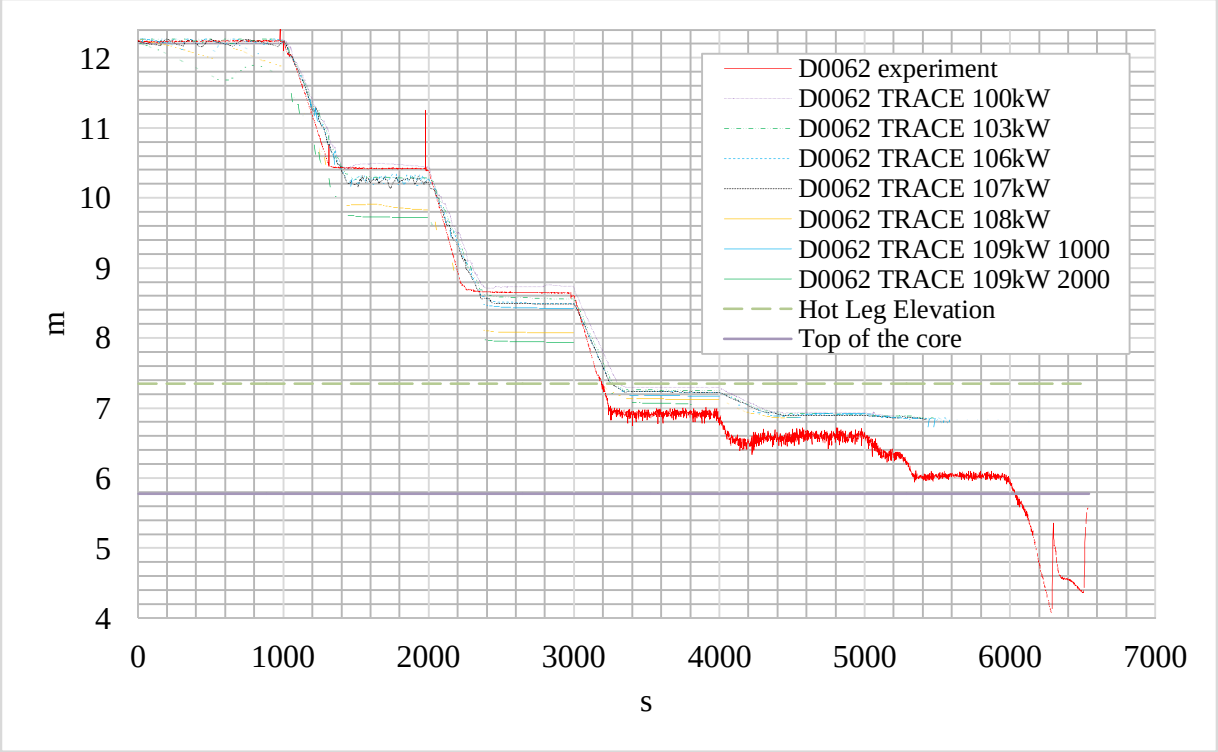

Figure 28: Simulation results versus experiment results, collapsed water level in the primary side, SIR-33 experiment

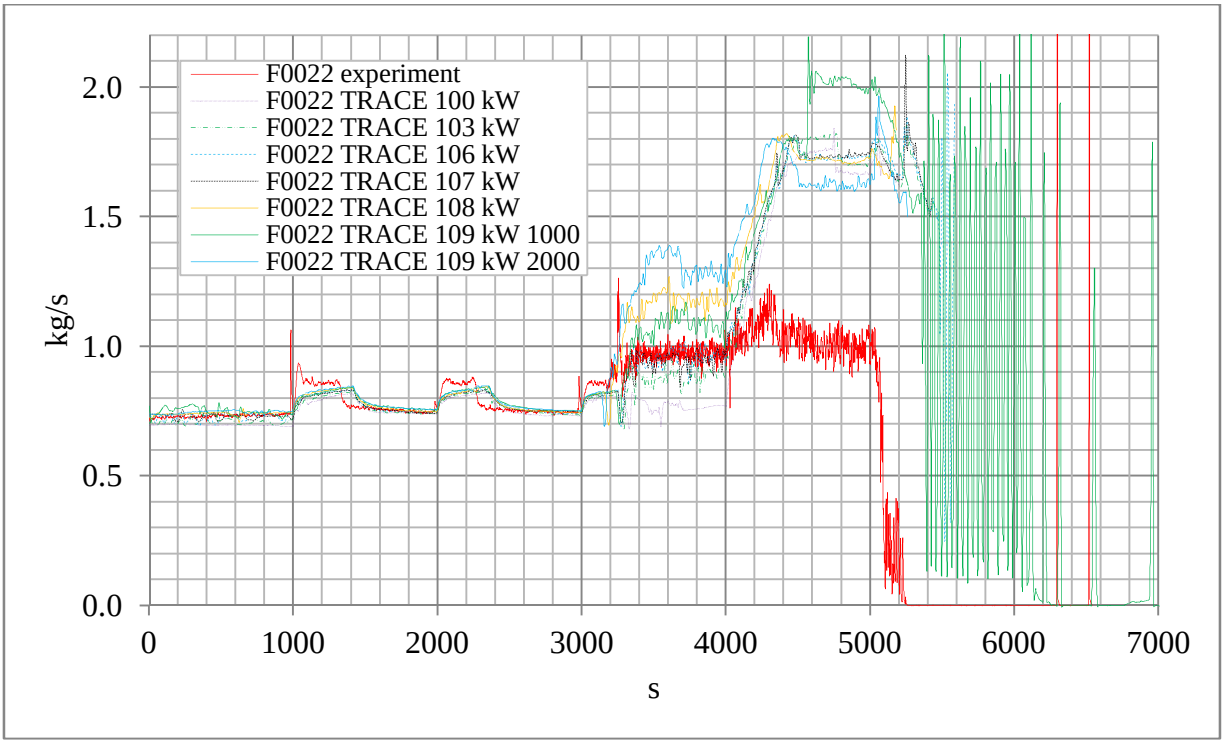

Figure 29: Simulation results versus experiments results, mass flow in loop II, SIR-33 experiment

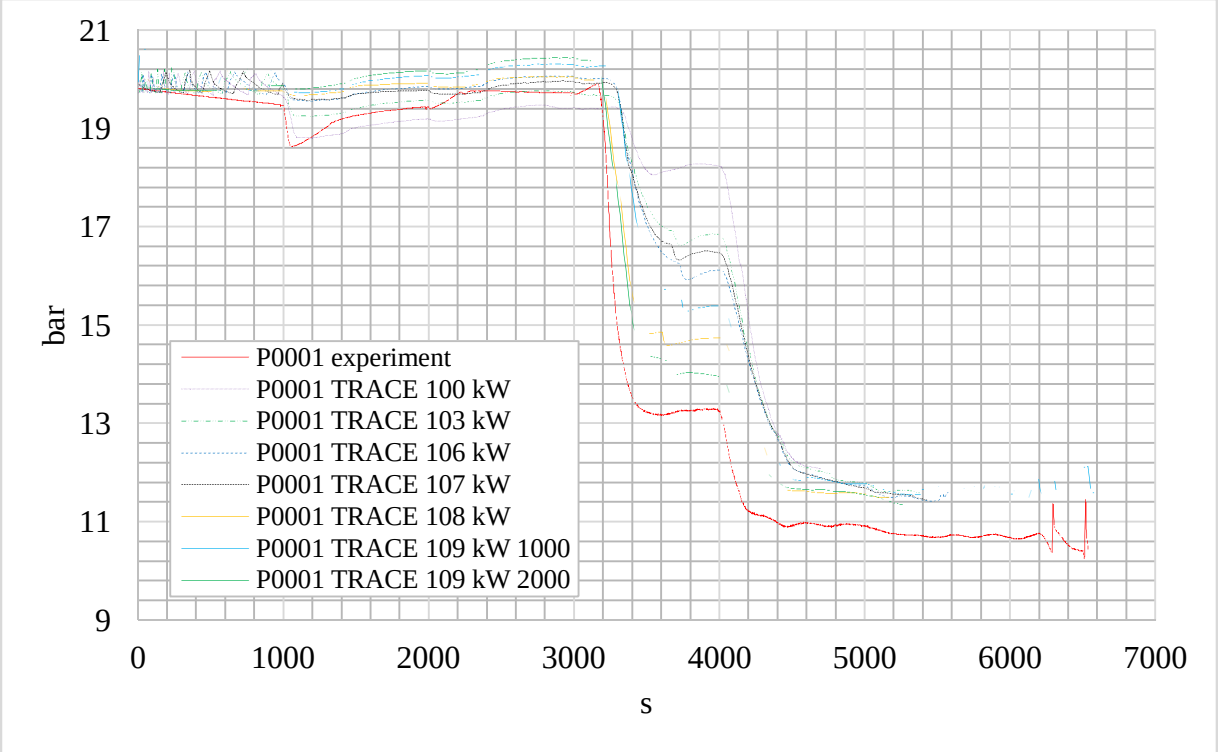

Figure 30: Simulation results versus experiment results, pressures in the primary and secondary side, SIR-33 experiment

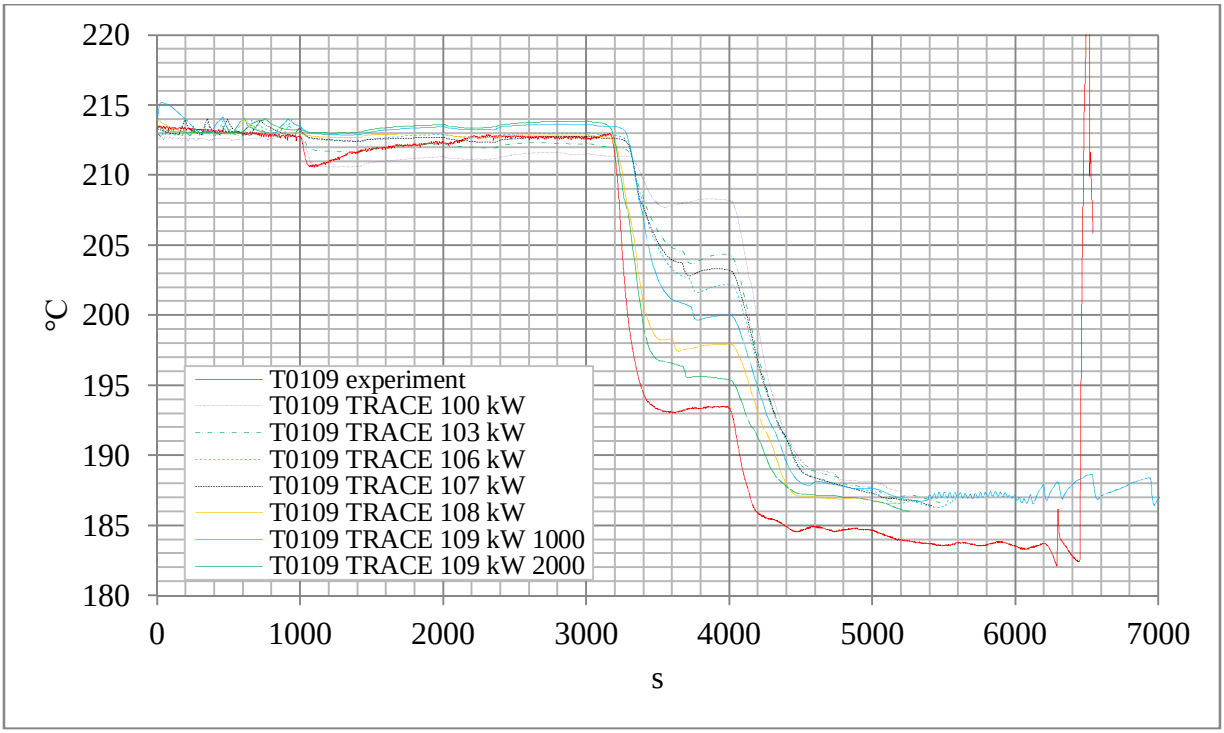

Figure 31: Simulation results versus experiment results, temperature in core outlet (channel A), SIR-33 experiment

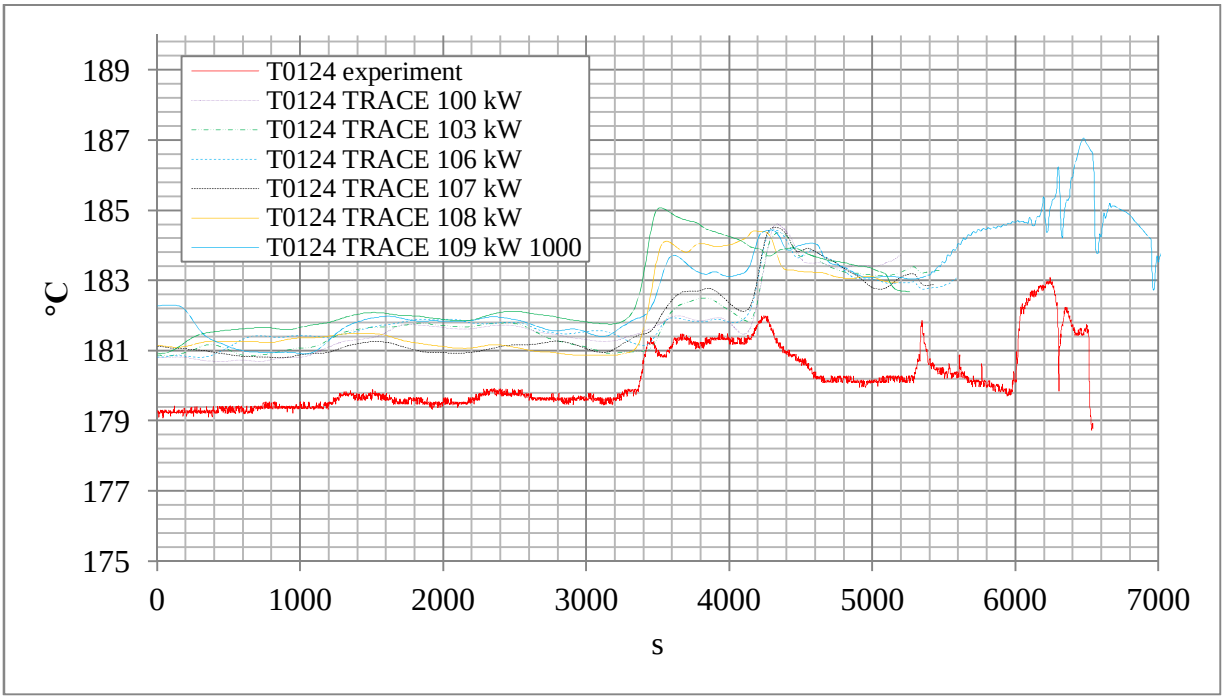

Figure 32: Simulation results versus experiment results, temperature in core inlet, SIR-33 experiment

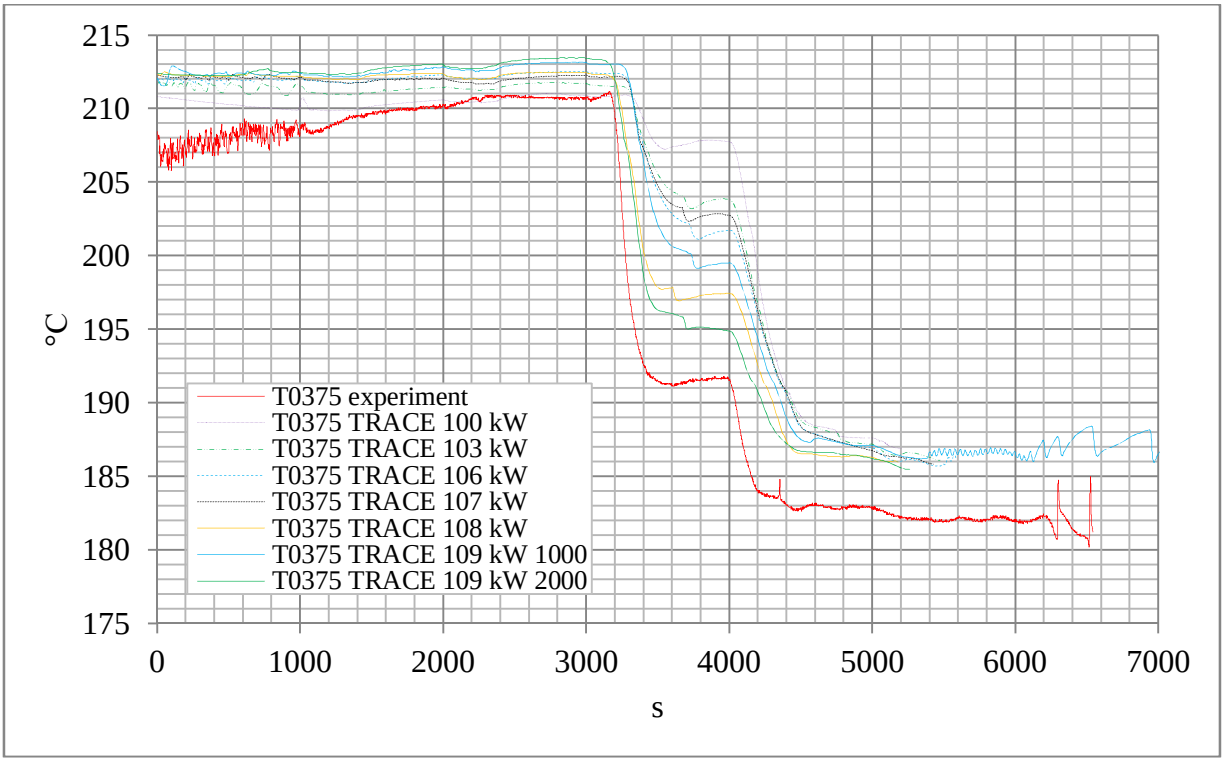

Figure 33: Simulation results versus experiment results, temperature in the bottom of the upper plenum, SIR-33 experiment

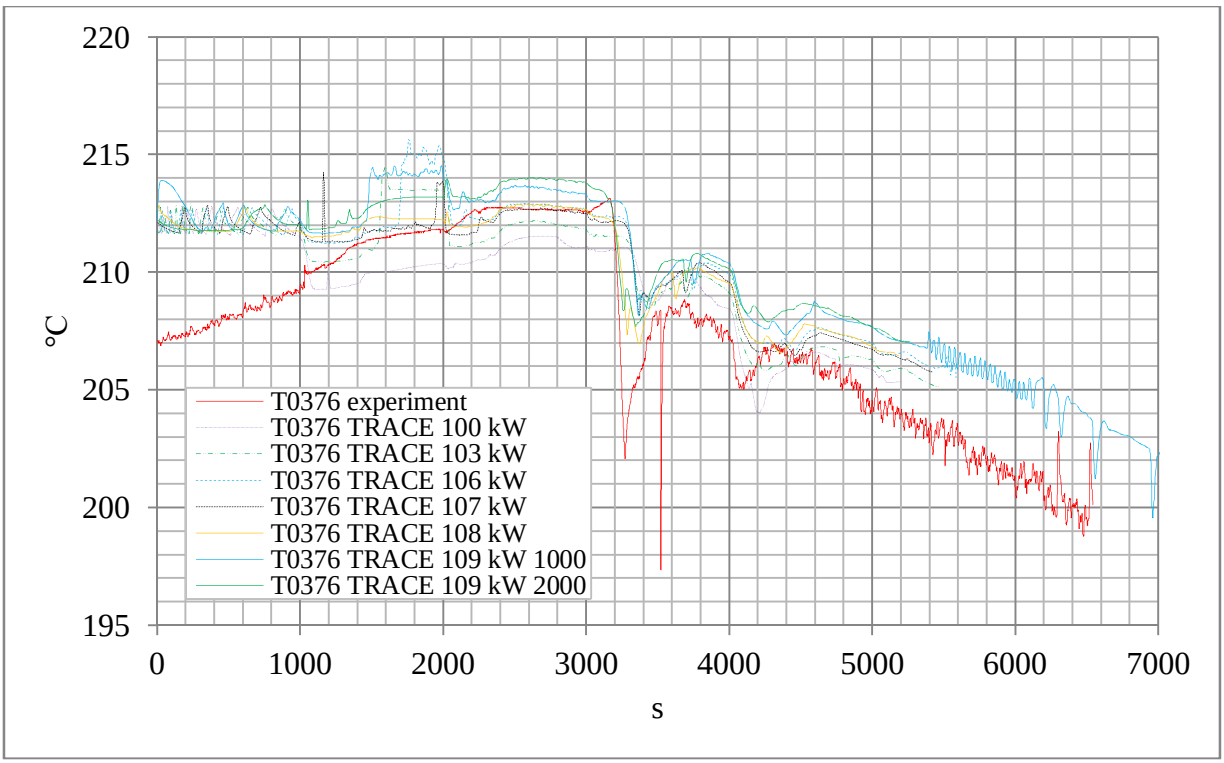

Figure 34: Simulation results versus experiment results, temperature in the top of the upper plenum, upper plenum top temperature is steam temperature, SIR-33 experiment

6.2. Small Break LOCA experiment

The small break LOCA experiment is very similar to the SIR experiments, but as far as the primary coolant now drains out steadily, results will not have most of sharp jumps in values. All basic processes inherent to this experiment are particularly the same as in the SIR experiments, thus they explained in details in chapter 6.1. The one important character is that now the working medium is draining out from upper part of the cold leg loop II.

6.2.1. SBL-50

Throughout the simulation, practically perfect matching of drained mass was achieved (Figure 39). Nevertheless, the collapsed water level functions do not coincide that precise. The angle of decrease for the experiment is more shallow (Figure 35). Because of such different inclinations, the moment when the collapsed water level falls below the hot leg connection elevation

comes at different time. Thus, there is a time delay between phenomena beginnings in the simulation and the experiment. This can be observed in every parameter of interest.

There is the natural circulation flow establishes within loops of the model, which can be concluded from mass flow rate functions (Figure 36-38). After 1000 seconds approximately, the simulation mass flow rate increases slightly in comparison to the experimental data. It might happen because of the primary pressure deeper drop at this moment (Figure 40). Consequently, it could cause more intense evaporation processes and by that increase the mass flow rate. After 4000 seconds, according to the experiment, the collapsed water level drops below the hot leg elevation and causes unhampered invasion of steam phase into the coolant flow. In its turn, that increases the mass flow rate, as long as the density difference of the working medium increases between upwards and downwards sides of the loop, as it was explained in chapter 6.1. Following to the experiment maximum possible flow rate occurs at the moment of 5000 seconds. On the other hand, the computational results slightly overestimated and the maximum occurs a bit earlier. It is worth to mention that simulation mass flow rate graphs are less smooth after 5000 seconds and have jumps, which is hard to explain.

Overall matching of the primary and secondary pressure along with temperatures is rather good. An interesting fact during the first drop of primary pressure between experiments SIR-31 and SBL-50 was found. In simulation of both experiments, the first drop is slightly lower than it happens according to the experiment. No clear explanation was found for this.

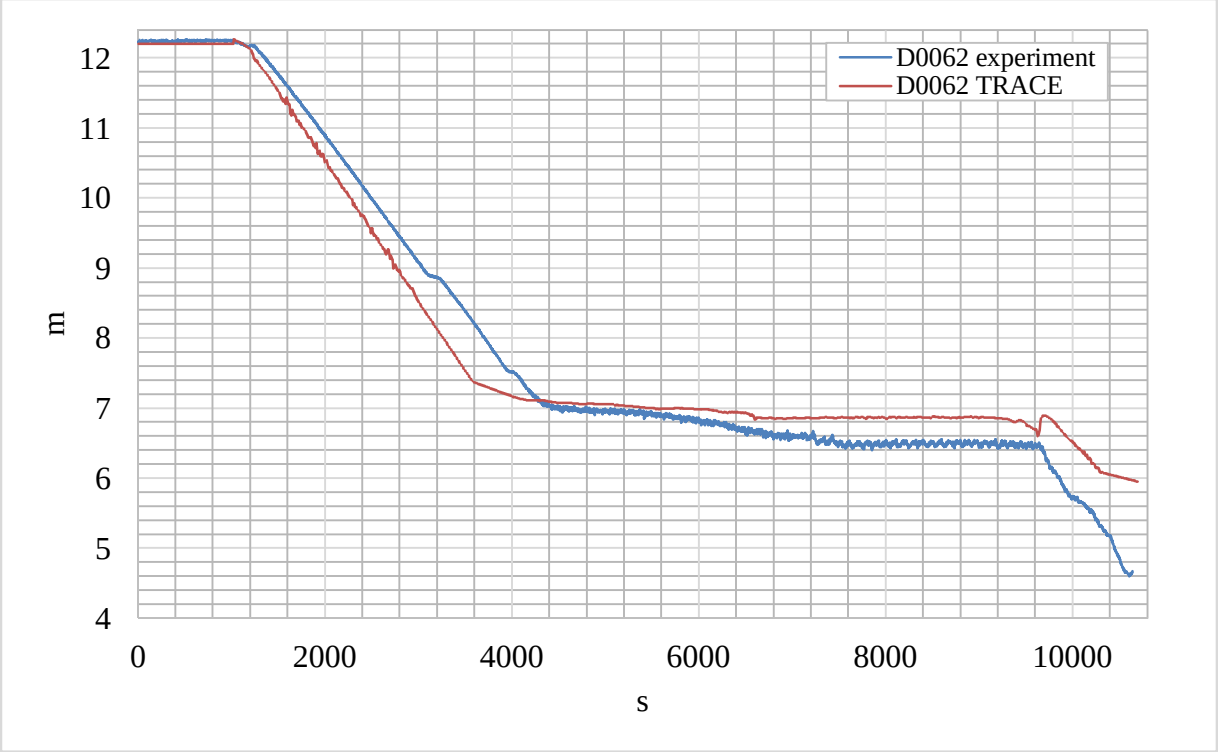

Figure 35: Simulation results versus experiment results, collapsed water level in the primary side, SBL-50 experiment

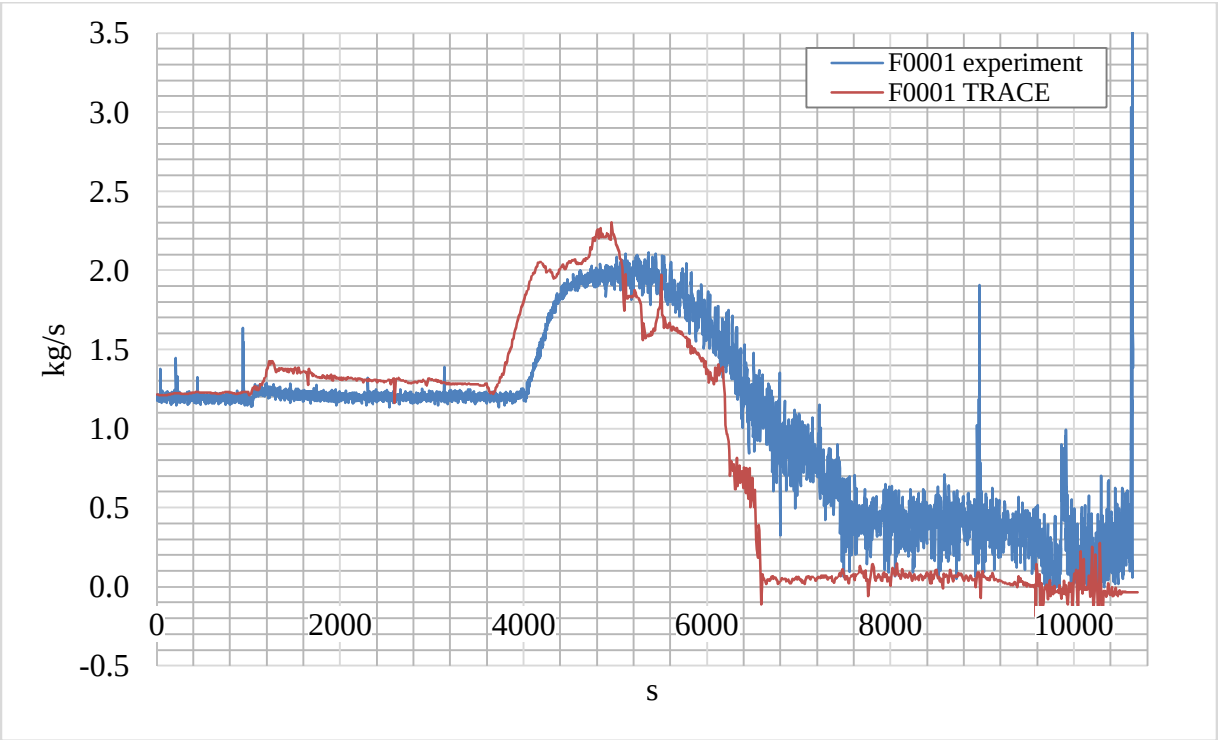

Figure 36: Simulation results versus experiment results, mass flow in the downcomer, SBL-50 experiment

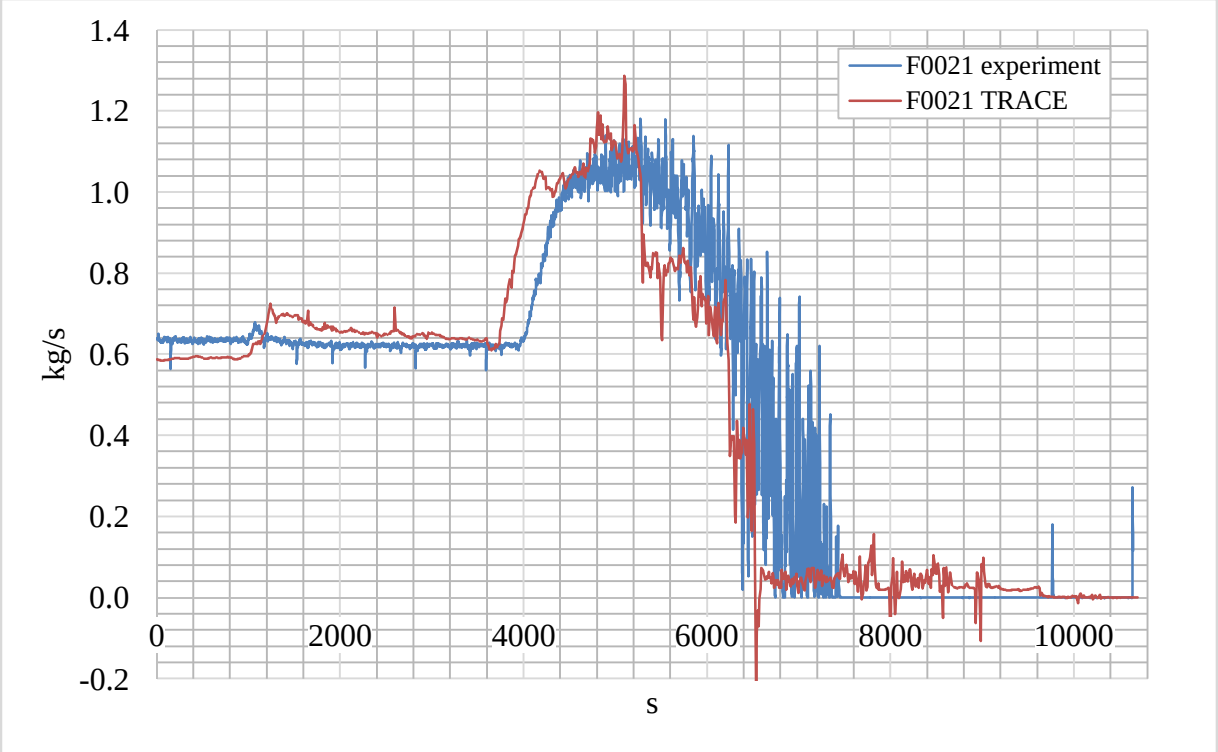

Figure 37: Simulation results versus experiment results, mass flow in loop I, SBL-50 experiment

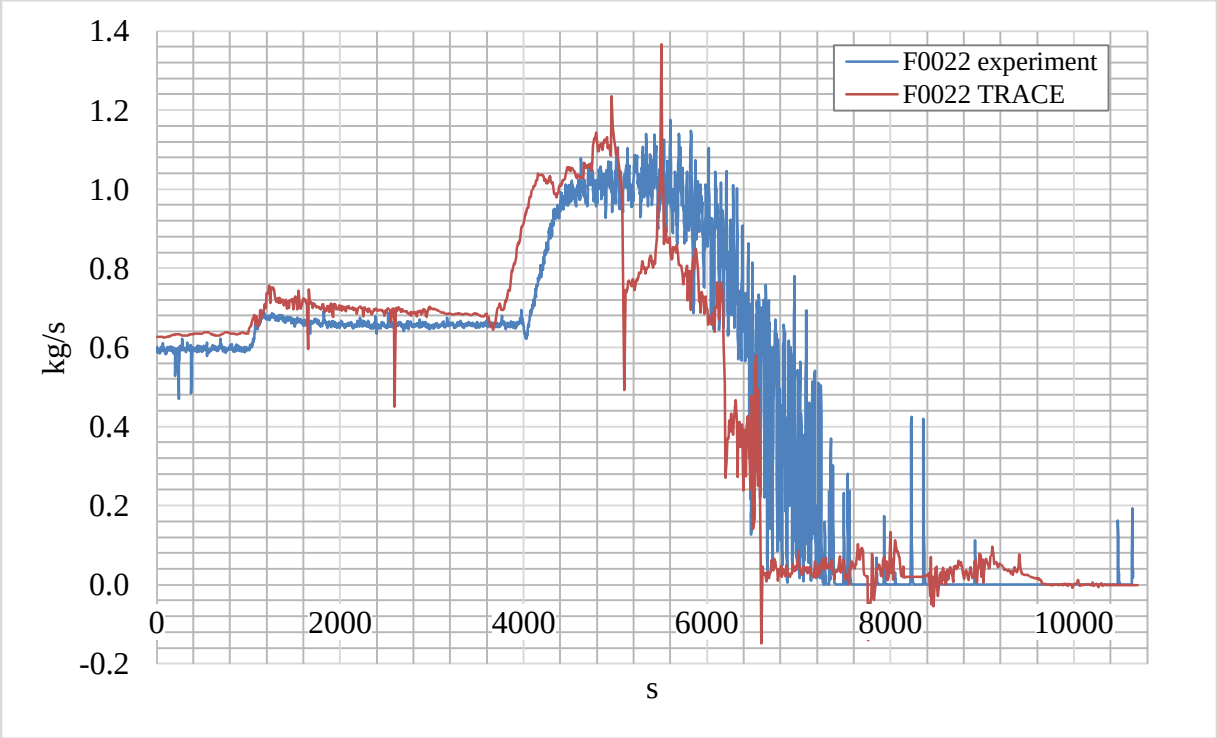

Figure 38: Simulation results versus experiment results, mass flow in loop II, SBL-50 experiment

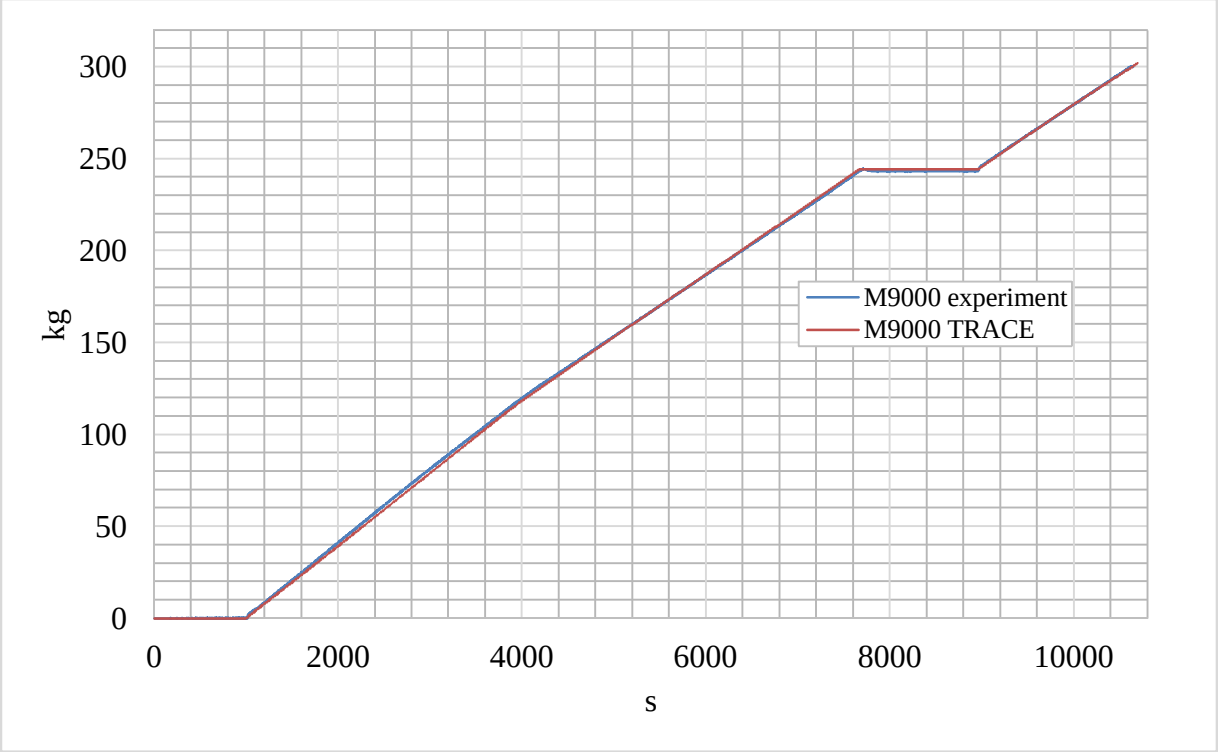

Figure 39: Simulation results versus experiment results, drained mass from the primary side, SBL-50 experiment

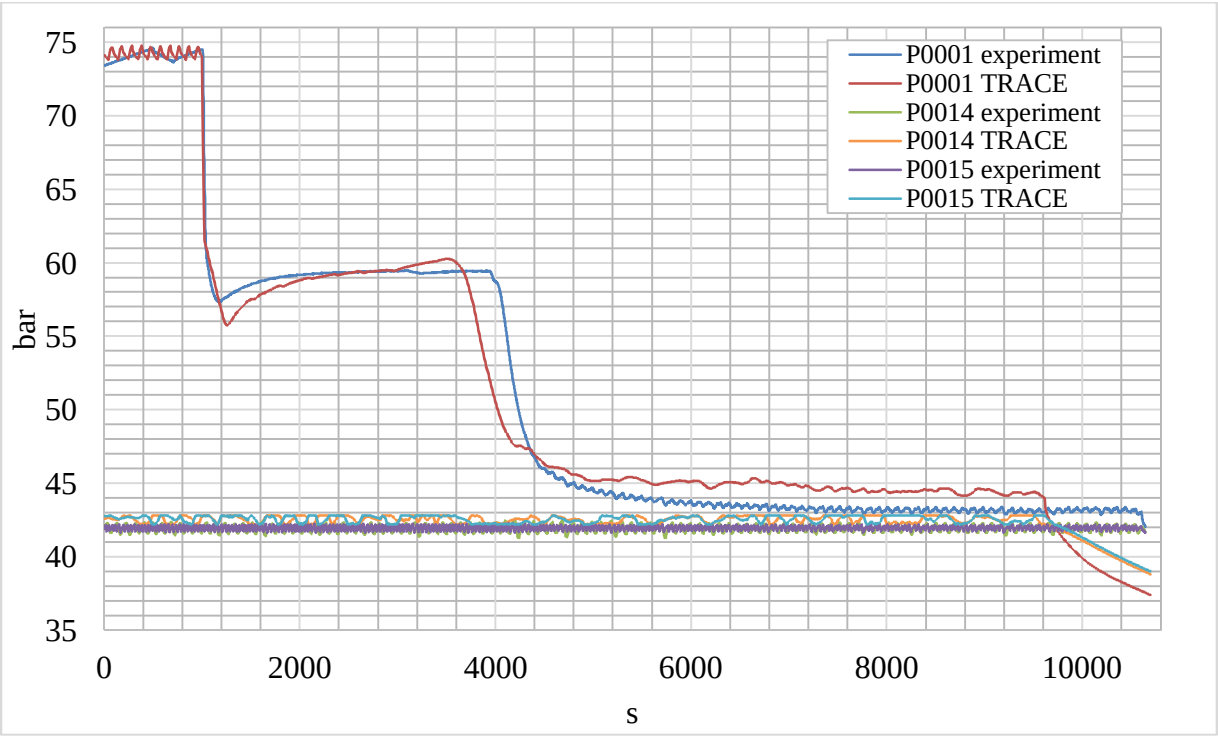

Figure 40: Simulation results versus experiment results, pressures in the primary and secondary side, SBL-50 experiment

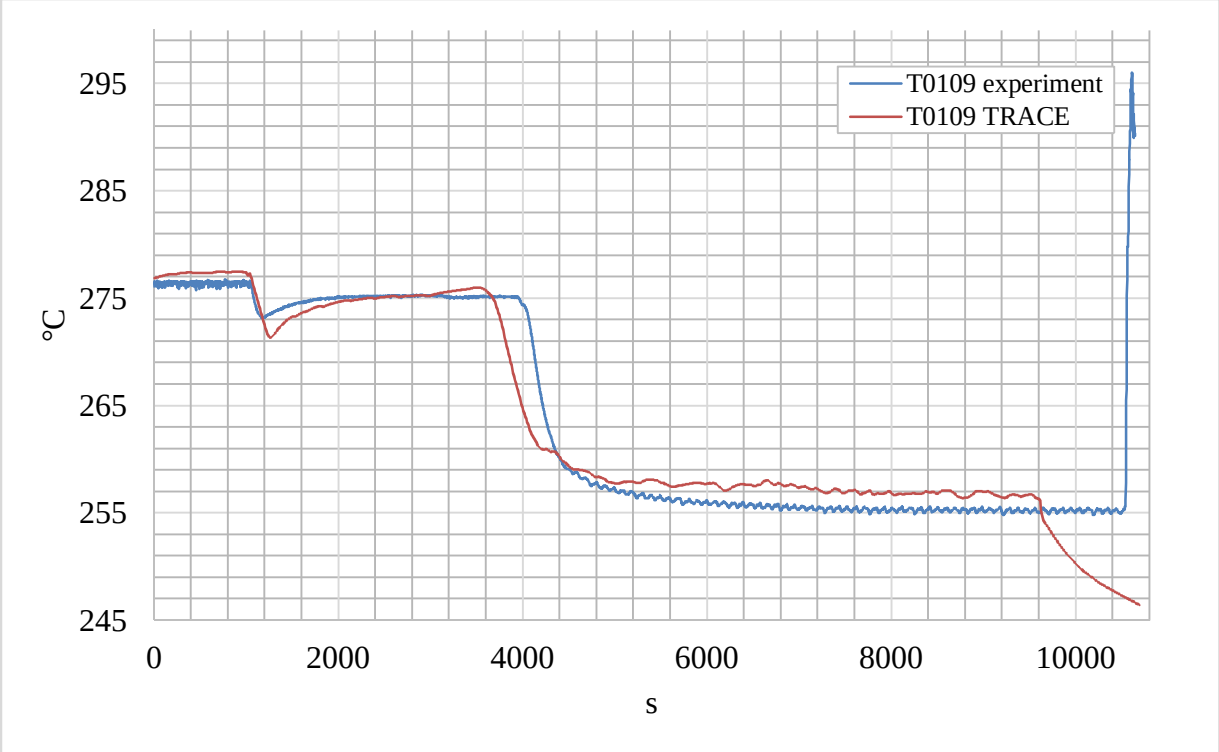

Figure 41: Simulation results versus experiment results, temperature in core outlet (channel A), SBL-50 experiment

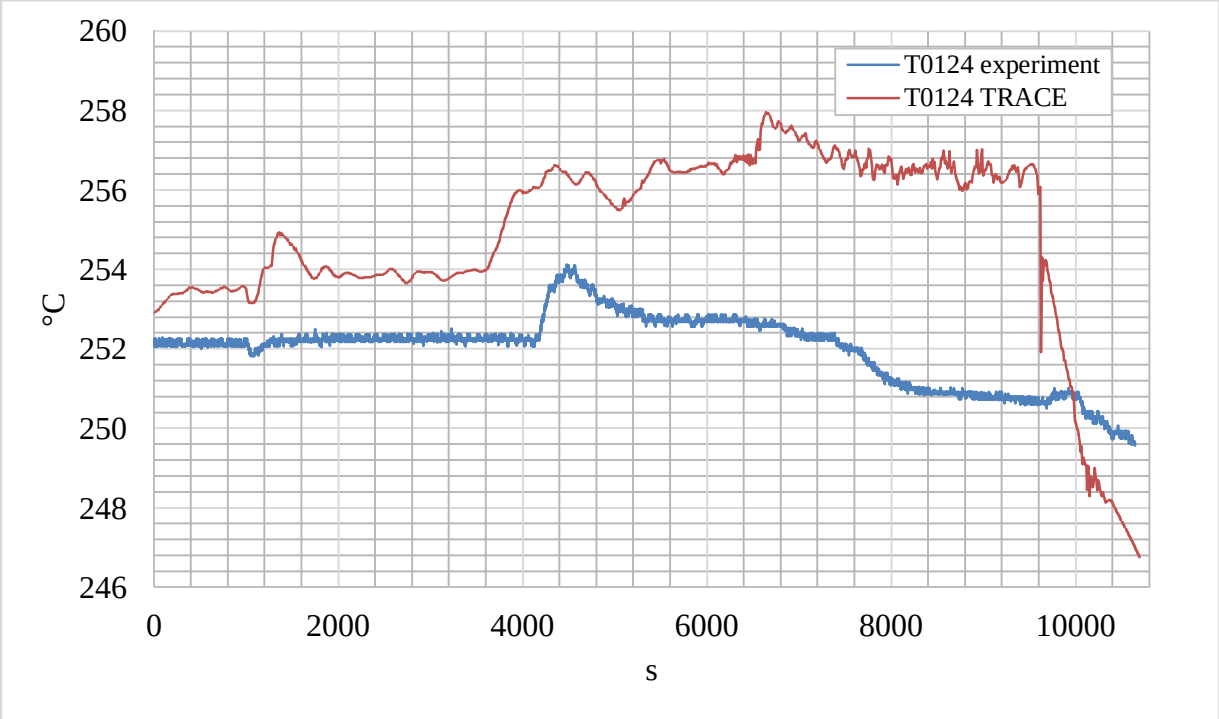

Figure 42: Simulation results versus experiment results, temperature in core inlet, SBL-50 experiment

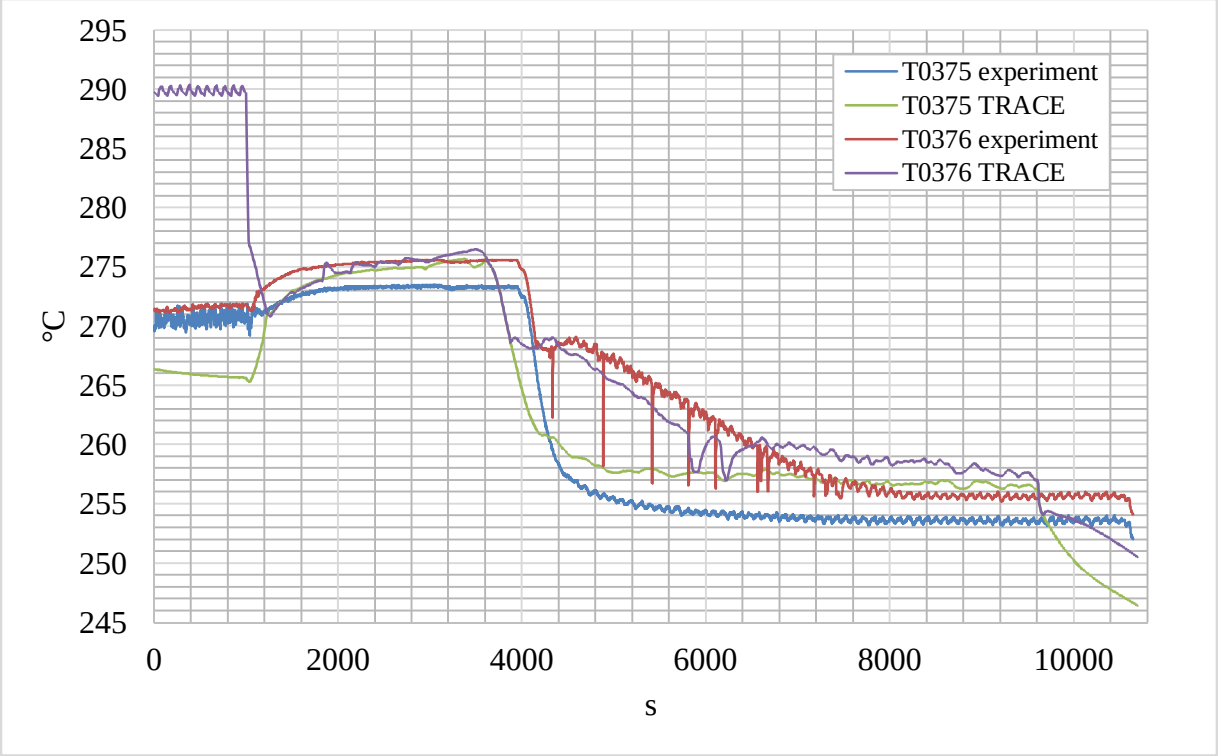

Figure 43: Simulation results versus experiment results, temperature in upper plenum (T0375 upper plenum bottom, T0376 upper plenum top), upper plenum top temperature is steam temperature, SBL-50 experiment

7 DISCUSSION AND CONCLUSIONS OF THE RESULTS

Throughout all four experiments that were computed with TRACE code it was possible to reach overall similarity between computational results and experiments data. In its turn, that allows us to state that the TRACE code possesses good enough ability for modelling such complicated and complex processes as thermal hydraulics of nuclear power plants. However, it does not allow us to trust such computational results blindly.

Thus, one of the most important and interesting parameters in these experiments was the amount of drained working medium. It was highly important to achieve as close similarity between experiment data and computational code as possible, because this particular function can be considered as a boundary condition to preserve, in order to be objective during analysis of the other parameters of the experiments. As it can be observed from Figure 13, 20, 27 during the acts of draining there is a slight inaccuracy particularly on every step of draining. This in the first look may be a problem of not totally correct frequency modelling as within the whole facility model as in the break element precisely. Thus, tuning of the break element frequency coefficient in the computational model allows to achieve better results in matter of conjunction between experimental and computed results. In case of the experiment SBL-50 (Figure 39), there were no complications faced in order to reach a good similarity between experimental data and calculations. Consequently, the conditions of the experiment itself are also very important aspect to take under consideration.

In all processed experiments the primary loop pressure functions obtained by computing are higher than those from experimental data. The tendency of this phenomenon makes to think that it most likely happens because of not accurate enough heat losses modelling to the environment. After 3000 seconds in all SIR experiments, a moment occurs when steam bubbles starts to be involved into the flow. This fact makes the torrent of working medium being a two phase flow. In its turn that adds more divergence between graphs of experimental pressure functions and computational pressure results. Even though the mathematical methods of two phase flow calculations are able to catch the basic phenomena of two phase flow thermal hydraulics, they are still not accurate enough. There is also an interesting drop of primary pressure observed in every SIR experiment, right after the first act of working medium drainage. It

is interesting because it drops out of the whole experiment picture. Thus, within the whole experiment there is an obvious tendency for the computational data to have overestimation for the primary pressure, though the first drop of pressure in every experiment is rather too deep, in comparison with experimental data. Unfortunately, the reasons of this drop are still hidden.

From explanations of numerous computational attempts with different conditions for SIR-33 in 6.3.1 one may conclude that steady state time is highly important to be long enough in order to eliminate possible errors or to indicate some problems related to a computational modal being built with TRACE code.

In conclusion, it can be stated that TRACE model of PWR PACTEL facility is objectively correctly designed. The model requires additional tunings, though overall performance is good enough. All important phenomena were observed within computational processing of experimental conditions.

BIBLIOGRAPHY

NUCLEAR REGULATORY COMMISSION. 2014. Federal register, 79(56), pp. 16106-16146.

BRUCE STEWART, H., 1979. Stability of Two-Phase Flow Calculation Using Two-Fluid Models. Journal of Computational Physics, (33), pp. 259-270.

BRUCE STEWART, H. and BURTON, W., 1984. Two-Phase Flow: Models and Methods. Journal of Computational Physics, (56), pp. 363-409.

HYVÄRINEN, J., 2015. A brief history of thermal-hydraulic system codes. Lecture notes distributed in Thermal Hydraulics of Nuclear Power Plants at Lappeenranta University of Technology, 2015 edn.

KOUHIA, V., RIIKONEN, V., PARTANEN, H., RÄSÄNEN, A., KAUPPINEN, O., TELKKÄ, J. and PYY, L., 2014. General description of the PWR PACTEL test facility - third edition. PAX 2/2014. Lappeenranta 2014: Lappeenranta University of Technology Nuclear Safety Research Unit.

KOUHIA, V., 2012. PACTEL and PWR PACTEL Test Facilities for Versatile LWR Applications. Science & Technology of Nuclear Installations, , pp. 1-8.

PURHONEN, H., 2006. PACTEL integral test facility - Description of versatile applications. Annals of Nuclear Energy, 33(11), pp. 994-1009.

RASMUSSEN, N.C., 1975. Der Rasmussen-Bericht (WASH-1400). Stellungnahmen zu Kernenergiefragen, .

U. S. NRC, 2007. TRACE V5.0 Theory manual: Equations, Solution Methods and Physical Models. . Volume 5 edn. Washington DC: NRC.

UNITED STATES NUCLEAR REGULATORY COMMISSION, 2015-last update, NRC: Backgrounder on the Three Mile Island Accident. Available: http://www.nrc.gov/reading-rm/doc-collections/fact-sheets/3mile-isle.html [4/15, 2015].